https://doi.org/10.5194/egusphere-2026-549
Preprint. Discussion started: 4 February 2026

A Memory-Based, non-Markovian, Linear Integro-Differential Equation for Root-Zone Soil Moisture

Mehdi Rahmati[1]

[1] Institute of Bio- and Geosciences: Agrosphere (IBG-3), Forschungszentrum Jülich, Germany

Correspondence to: Mehdi Rahmati (mehdirmti@email.com; m.rahmati@fz-juelich.de)

Abstract. Soil-moisture memory (SMM) regulates the evolution of drought, hydrological predictability, and land–atmosphere coupling, yet many conventional diagnostic metrics simplify this complex phenomenon into a sole memory timescale. In this paper, we introduce a unified observation-driven framework — a scale-aware Linear Integro-Differential Equation (LIDE) for root-zone soil moisture — which quantifies the accumulation of memory at different timescales, e.g., fast memory (τ_F) and slow memory with very-short-term (τ_{VSS}), short-term (τ_{SS}), mid-term (τ_{MS}), and long-term (τ_{LS}) components as well as an additional memory saturation timescale (τ_{Sat}). A helper function, namely Logit–Piecewise Memory Segmentation (LPMS) method, is also developed which automates the timescales detection. When applied to lysimeter-based in-situ daily-based observations from three different hydro-climatic regimes in Germany lasting for 2013 to 2018, LIDE reveals a τ_F timescale from ~3–32 days and τ_{SS}, τ_{MS}, and τ_{LS} timescales from ~13-39, ~115–127, and ~218–541 days, respectively, and a theoretical τ_{Sat} timescale from ~9-15 years, while the τ_{VSS} remained undetectable. On top of the multi-timescales' quantification, LIDE also provides additional quantitative information about memory strength, as assessed by actual memory capacity ($\mathcal{K}_{Sat}$), which is not available through conventional diagnostic metrics; with $\mathcal{K}_{sat}$ being relatively constant over the examined sites (1.12–1.24 days^{-1}). The integrated kernel also allows to retrieve the oscillatory saturation dynamics associated with soil-moisture reemergence from observations for the first time. Applying LIDE to hourly, daily, and monthly data reveals its scale-aware nature, whereas when applied to hourly data, it provides additional timescales (e.g., sub-daily τ_F and τ_{VSS} timescales), while when applied to coarser data, it smooths them out. Collectively, obtained results place LIDE as a state-of-the-art and state-of-the-practice approach in quantifying SMM characteristics that are physically interpretable and scalable and can greatly advance drought sciences, ecohydrology and land-surface modeling.

1. Introduction

Soil moisture memory (SMM) — the soil's ability to retain information about past trajectories — a frequently analyzed component of soil memory (Rahmati, Or, et al., 2023) — is an important characteristic of soil moisture dynamics that influences its interaction with key land surface processes, such as geochemical, hydrological, and biome-related processes. SMM is a combined response to 1) forcing anomalies such as variability in rainfall, evapotranspiration, heatwaves, and droughts, 2) alterations in soil system initiated by land use changes and soil management, and 3) anthropogenic or natural changes in soil system properties such as soil structure, soil pore size distribution, or conductivity (Rahmati et al., 2024). The

https://doi.org/10.5194/egusphere-2026-549
Preprint. Discussion started: 4 February 2026

SMM is traditionally characterized by using classical time series analysis under the assumption of so-called component model for soil moisture evolution, either by e-folding method (Delworth and Manabe, 1988; Hasselmann, 1976; Koster and Suarez, 2001) — capturing only one e-folding timescale — or the hybrid stochastic-deterministic model (McColl et al., 2019) — decomposing the single value in e-folding method into two different timescales, namely short- and long-term SMM timescales. Although several other metrics is also introduced to quantify SMM timescale (see the full list of methods in Rahmati et al., 2024), the main concept remains the same as that of the above methods in that it captures only one SMM timescale, or at most two with the state-of-the-art hybrid stochastic-deterministic modelling method (McColl et al., 2019). However, characterizing SMM as single or even double characteristic timescales is inadequate to reflect the complexities of soil moisture dynamics in natural systems. Soil moisture is the average of processes running at quite different modes such as rapid atmospheric forcing, root-zone processes and preferential flow and slower sub-surface storage and recharge, which can potentially lead to memory accumulation at different timescales. Therefore, by restricting memory representation to a single or two parameters, the system is oversimplified and potential information on its temporal behavior under different hydroclimatic conditions may be lost.

As an alternative, we hypothesize that exploring the dynamics of soil moisture through application of the projection formalism of the Mori–Zwanzig theory (Falkena et al., 2019; Mori, 1965; Zwanzig, 1973) could enable us to distinguish between fast and slow processes involved in soil moisture evolution and detect its possible memory components acting at different timescales. This is based on the fact that, through applying the model reduction approach of the Mori–Zwanzig formalism, a fully resolved deterministic dynamical system (e.g., the spatiotemporal evolution of soil moisture over a layered or discretized soil profile) can be transformed into a stochastic dynamical system for the system's observable(s) of interest (e.g., root-zone soil moisture, θ_{root}, only). This stochastic dynamical system will still capture the full dynamics of the system and is not an approximation (Falkena et al., 2019). In this way, the hidden dynamics of 'irrelevant' or ‘unobserved’ degrees of freedom (e.g., soil moisture evolution in surface layer or deeper layers) are incorporated into memory kernels and occasionally into fast-fluctuating residual forces, also known as noise term. Due to the stochastic nature of the reduced system, its parameters (namely the memory kernel and the noise term) can be obtained numerically, provided that the variable of interest (e.g., θ_{root} in our case) is observed sufficiently regarding the observation period and observation intervals. The determined memory kernel, then, enables us to explore memory accumulation at different timescales, which can lead to the quantification of SMM multi-timescales. In this paper, under this postulation, we therefore apply the Mori–Zwanzig model reduction approach to a stratified soil profile comprising three layers (see Fig. 1): 1) a shallow surface layer with a depth of less than 5 cm, 2) the root zone, which comprises the active soil layer on which plant life relies, and 3) the deep vadose zone, the deeper layer below the root zone that acts as a link between the root zone and groundwater. The main objective of this paper is therefore to apply the Mori–Zwanzig formalism to develop a Linear Integro-Differential Equation (LIDE) for θ_{root} only, which would allow us to quantify SMM at different timescales without worrying about the evolution of soil moisture in the surface and deeper layers while their effects are still present and accounted.

The development of LIDE will enable us to quantify the accumulation of memory at different timescales, e.g., fast memory (τ_F) and slow memory with very-short-term (τ_{VSS}), short-term (τ_{SS}), mid-term (τ_{MS}), and long-term (τ_{LS}) components as well as

https://doi.org/10.5194/egusphere-2026-549
Preprint. Discussion started: 4 February 2026

memory saturation timescale (τ_{Sat}), which is detailed in upcoming section. Such multiscale SMM identification is important because different memory modes control fundamentally distinct processes and feedback. Fast memory (days to weeks) plays, for example, a critical role for runoff generation and flood risk assessments. Short-term slow memory (days to months) is probably crucial for land–atmosphere coupling and flash-drought evolution (e.g., soil-moisture anomalies lead to extreme drought warning; Liang and Yuan, 2021). Mid-term slow-memory (months to seasons) drives vegetation resilience, soil–plant water use, and ecosystem carryover (Groh et al., 2020). Long-term memory (seasons to years or decades) is nested in the deep soil and groundwater stores affecting persistence of hydrological drought character (Farmani et al., 2025). Therefore, identifying and capturing these distinct timescales increases the realism of climate models, as well as the skill of drought forecasts and our understanding of resilience in coupled ecohydrological systems.

In the following sections, we will first present the theoretical background to the development of LIDE as well as automation of its memory kernel analysis through LPMS method. We will then use LIDE to capture SMM characteristics in Germany under three different hydrological conditions, based on state-of-the-art weighable lysimeter data. The SMM characteristics provided by LIDE will then be compared with the classical metrics introduced in the literature. Finally, we will examine the usability and consistency of the LIDE framework when applied to data with different measurement time intervals. Finally, the strengths and weaknesses of the LIDE framework are presented, along with possible future research directions.

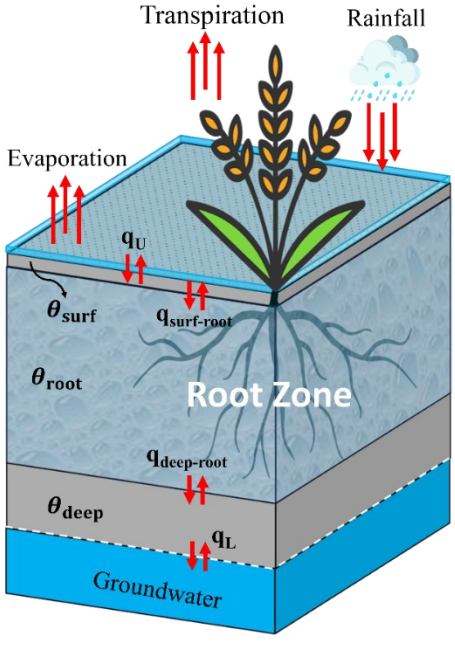

Figure 1: Soil profile with three layers, including the surface layer and root and vadose zones, coupled by flow densities (q).

https://doi.org/10.5194/egusphere-2026-549
Preprint. Discussion started: 4 February 2026

2. Introduction

2.1. LIDE Development

The time evolution of soil moisture, θ, for a three-layer soil profile (shown in Fig. 1) can be described by applying a system of coupled ordinary differential equations (ODEs) of layer-average moisture contents in the surface soil (θ_{surf}), root zone (θ_{root}), and deeper vadose zone (θ_{deep}):

$$\frac{d\boldsymbol{\theta}(t)}{dt} = \boldsymbol{R}\big(\boldsymbol{\theta}(t)\big) \qquad \text{with} \qquad \boldsymbol{\theta}(t=0) = \boldsymbol{\theta_0} \tag{1}$$

where t is time [T], $\boldsymbol{R}\big(\boldsymbol{\theta}(t)\big) = \Big(R_{\mathrm{surf}}\big(\boldsymbol{\theta}(t)\big), R_{\mathrm{root}}\big(\boldsymbol{\theta}(t)\big), R_{\mathrm{deep}}\big(\boldsymbol{\theta}(t)\big)\Big) \in \mathbb{R}^{n=3}$ [T^{-1}] is a vectorized nonlinear functions of $\boldsymbol{\theta}$ [L^3L^{-3}] with $\boldsymbol{\theta} = (\theta_{surf}, \theta_{root}, \theta_{deep}) \in \mathbb{R}^{n=3}$ and initial conditions of $\boldsymbol{\theta}_0 = (\theta_{0,\,surf}, \theta_{0,\,root}, \theta_{0,\,deep}) \in \mathbb{R}^{n=3}$. Classically, one can obtain the nonlinear functions of $R_{surf}(\boldsymbol{\theta})$, $R_{root}(\boldsymbol{\theta})$, and $R_{deep}(\boldsymbol{\theta})$ by integrating the Richards-Richardson equation (RRE) (Richards, 1931; Richardson, 1922) for different depths corresponding to the upper and lower boundaries of each layer in three-layered profile (Fig. 1). The RRE governing equation for vertical movement of water in soils reads as below:

$$\frac{d\theta(t)}{dt} = -\frac{dq(t)}{dz} - S(t) \tag{2}$$

with z [L] being the vertical coordinate, positive downward, $q(t)$ the vertical water flow density [LT^{-1}] and $S(t)$ [T^{-1}] the source/sink term (i.e., root water uptake).

The layer-wised integration of RRE can lead to a soil-centered mechanistic modeling approach with one ODE for each layer: three ODEs in total. The ODEs obtained should be solved simultaneously (i.e. in a coupled manner) to describe the temporal evolution of θ for the entire profile, even though, in most cases, only one variable is of interest (e.g., θ_{root}). Alternatively, we propose applying the formal model reduction approach introduced by Mori (1965) and Zwanzig (1973). Such application would transform the fully resolved deterministic dynamical system defined in Eq. (1) into a stochastic dynamical system for θ_{root} only. To do this, we simplify the nonlinear system of coupled ODEs defined in Eq. (1) as linear systems of coupled ODEs, as below:

$$\frac{d\theta_{\mathrm{surf}}(t)}{dt} = \lambda_{\mathrm{s}}\theta_{\mathrm{surf}}(t) + \beta_{\mathrm{r}\to\mathrm{s}}\theta_{\mathrm{root}}(t) + \varepsilon_{\mathrm{s}}(t) \tag{3}$$

$$\frac{d\theta_{\mathrm{root}}(t)}{dt} = \lambda_{\mathrm{r}}\theta_{\mathrm{root}}(t) + \beta_{\mathrm{s}\to\mathrm{r}}\theta_{\mathrm{surf}}(t) + \beta_{\mathrm{d}\to\mathrm{r}}\theta_{\mathrm{deep}}(t) + \varepsilon_{\mathrm{r}}(t) \tag{4}$$

$$\frac{d\theta_{\mathrm{deep}}(t)}{dt} = \lambda_{d}\theta_{\mathrm{deep}}(t) + \beta_{r\to d}\theta_{\mathrm{root}}(t) + \varepsilon_{d}(t) \tag{5}$$

where λ denotes the intrinsic decay timescale in each layer (noted by the subscripts s for the surface layer, r for the root zone, and d for the deep vadose layer), β denotes the coupling effects, indicated by the direction of the arrows, and ε denotes the noise terms that account for the unresolved dynamics that emerge from the linearity assumption as well as possible forcings not considered through λ and β — e.g., precipitation in the case of surface layer. To solve the above coupled system directly for relevant observable variable θ_{root} only while considering the effect of irrelevant variables θ_{surf} and θ_{deep}, we can solve Eq. (3) and (5) for the irrelevant variables (θ_{surf} and θ_{deep}) assuming known knowledge on θ_{root} and the noise terms (Gouasmi et al., 2017):

https://doi.org/10.5194/egusphere-2026-549
Preprint. Discussion started: 4 February 2026

$$\theta_{\text{surf}}(t) = \theta_{0,\text{surf}}\, e^{\lambda_s(t-t_0)} + \beta_{r\to s}\int_{t_0}^{t} e^{\lambda_s(t-\tau)}\theta_{\text{root}}(\tau)d\tau + \int_{t_0}^{t} e^{\lambda_s(t-\tau)}\varepsilon_s(t)d\tau \quad (6)$$

$$\theta_{\text{deep}}(t) = \theta_{0,\text{deep}}\, e^{\lambda_d(t-t_0)} + \beta_{r\to d}\int_{t_0}^{t} e^{\lambda_d(t-\tau)}\theta_{\text{root}}(\tau)d\tau + \int_{t_0}^{t} e^{\lambda_d(t-\tau)}\varepsilon_d(t)d\tau \quad (7)$$

By replacing Eq. (6) and (7) in Eq. (4) and further rearranging it, the LIDE framework for the relevant variable, θ_{root}, can be obtained as below:

$$\frac{\partial\theta_{root}(t)}{\partial t} = \lambda\theta_{\text{root}}(t) + \int_{t_0}^{t} K(\tau)\theta_{\text{root}}(t-\tau)d\tau + F(t) \quad (8)$$

where t_0 is the initial time where the θ_{root} is observed (usually being set to zero), τ is an integral variable defining the lag values [T], λ is the frequency coefficient [T^{-1}], K is the memory kernel [T^{-2}] which provides feedback of surface layer and deep vadose zone on θ_{root} over time, $F(t)$ is the noise term [T^{-1}] (Falkena et al., 2019; Gottwald et al., 2016). The memory kernel $K(\tau)$ and noise term $F(t)$ of LIDE framework are defined as below:

$$K(\tau) = \beta_{s\to r}\beta_{r\to s}e^{\lambda_s(t-\tau)} + \beta_{d\to r}\beta_{r\to d}e^{\lambda_d(t-\tau)} \quad (9)$$

$$F(t) = \emptyset(t) + \omega(t) + \varepsilon_r(t) \quad (10)$$

where ∅(t) is the evolution of initial conditions of surface and deep vadose layers, and ω(t) is convolutions of forcings — e.g., precipitation through ε_s(t), see Eq. (6), and groundwater contribution through ε_d(t), see Eq. (7) — defined as below (the remaining parameters are defined as before):

$$\emptyset(t) = \beta_{s\to r}\theta_{0,\text{surf}}\, e^{\lambda_s(t-t_0)} + \beta_{d\to r}\theta_{0,\text{deep}}\, e^{\lambda_d(t-t_0)} \quad (11)$$

$$\omega(t) = \int_{t_0}^{t}\beta_{s\to r}e^{\lambda_s(t-\tau)}\varepsilon_s(t)d\tau + \int_{t_0}^{t}\beta_{d\to r}e^{\lambda_d(t-\tau)}\varepsilon_d(t)d\tau \quad (12)$$

Applying the above reduction procedure, we have now reduced the nonlinear ODE systems in Eq. (1) to a single expression for the relevant variable, θ_{root}, in Eq. (8), which depends on its intrinsic decay of θ_{root}, coupling effects of surface and deeper layers through memory kernel, as well as stochastic noise term. This reduced system defined by the Mori-Zwanzig equation, hereafter called LIDE, is equivalent to the full system and exhibits the same behavior (Falkena et al., 2019) and is not an approximation (Gottwald et al., 2016). It is in the form of a generalized Langevin equation (Gottwald et al., 2016) as the right-hand side comprises three different terms, each of which relates to the Markov term, the memory term, and the noise term, respectively (Falkena et al., 2019; Gottwald et al., 2016). In simple notation, we can rewrite the LIDE as below:

$$\frac{\partial\theta_{root}(t)}{\partial t} = \lambda\theta_{\text{root}}(t) + \{K * \theta_{\text{root}}\}(t) + F(t) \quad (13)$$

where "∗" represents a convolution between the memory kernel and θ_{root}. Departing from current state-of-the-art Markovian-based reduced-order models of θ_{root} (e.g., Delworth and Manabe, 1988; Koster and Suarez, 2001; McColl et al., 2019; Seneviratne et al., 2010), our LIDE framework incorporates an essential memory term, derived from a memory kernel $K(\tau)$, that accounts for the trajectories of θ_{root} by bringing in the feedback from surface and deeper layers. This innovation allows the

https://doi.org/10.5194/egusphere-2026-549
Preprint. Discussion started: 4 February 2026

model to realistically capture the non-linear, time-dependent responses of θ_{root} to extreme events, although it is formalized in linear form.

2.2. Numerical Solution of LIDE

One can solve the proposed LIDE model and determine it parameters — namely λ, $K(\tau)$, and $F(t)$ — numerically according to Schmitt and Schulz (2006) given that the measured θ_{root} data is available. Briefly, to solve the LIDE model introduced in Eq. (8), one needs to rewrite it in the form of autocorrelation function as below (Schmitt and Schulz, 2006):

$$\frac{\partial \rho(t)}{\partial t} = \lambda \rho(t) + \int_{t_0}^{t} K(\tau)\, \rho(t) d\tau \tag{14}$$

Doing this, the noise term vanishes due to averaging as the standard property of the Mori-Zwanzig equation derived from the projection. The derivation in Eq. (14) assumes stationarity and existence of the ensemble average. Therefore, instead of solving the LIDE for θ_{root}, we solved it for $\Delta\theta_{root} = \theta_{root}(t) - \theta_{root}(t-1)$. To determine the parameters of the Eq. (14), Schmitt and Schulz (2006) suggested a corresponding time-ordered discrete version of the Eq. (14) as below:

$$\rho[t] - \rho[t-1] = -\sum_{i=0}^{t-1} K[t-i-1]\rho[i] \tag{15}$$

The above equation can easily be solved for $K[t]$ having $\rho[t]$ known from θ_{root} time series. Like Eq. (15), one can also write the time-ordered discrete form of the Eq. (8) as below (Schmitt and Schulz, 2006):

$$\theta_{root}[t] - \theta_{root}[t-1] = -\sum_{i=0}^{t-1} K[t-i-1]\theta_{root}[i] + F[t-1] \tag{16}$$

Therefore, we can calculate F[t] from known θ_{root} time series as well as $K[t]$ determined as above. It should be noted that with Eq. (15), the parameter λ is incorporated into $K[0]$ which can be separated as below:

$$\lambda = \widetilde{K}[0] - K[0] \tag{17}$$

where $\widetilde{K}[t]$ is defined as below:

$$\widetilde{K}[t] = \frac{1}{\langle \theta_{root}^2 \rangle(0)} \langle F[t_0] | F[t-t_0] \rangle_{t_0} \tag{18}$$

where $\langle \theta_{root}^2 \rangle(0)$ is the variance of the θ_{root} time series and $\langle F[t_0] | F[t-t_0] \rangle_{t_0}$ represents the conditional expectation for LIDE-reconstructed noise term, at time t_0, given its value a lag t. However, in practice, we cannot directly compute this from a single finite time series. Following standard practice, therefore, the conditional expectation is approximated by a time-averaged estimate which relies on second-order statistics, assuming weak stationarity and ergodicity of the noise process. Therefore, in practice, we use following approximation to calculate $\widetilde{K}[t]$:

$$\widetilde{K}[t] = \frac{1}{\langle \theta_{root}^2 \rangle(0)} \begin{cases} \gamma_f(0), & t = 1 \\ \dfrac{1}{t-1} \displaystyle\sum_{\ell=1}^{t-1} \gamma_f(\ell), & t \geq 2 \end{cases} \tag{19}$$

where $\gamma_f(\ell)$ is autocovariance of noise term at lag ℓ. In ideal cases, the $\widetilde{K}[t]$ and $K[t]$ are equal except for their first elements.

https://doi.org/10.5194/egusphere-2026-549
Preprint. Discussion started: 4 February 2026

2.3. LIDE-driven Multiscale Memory Regimes Identification

The λ and $K(\tau)$ parameters of LIDE contain memory information of the system and one can explore them to identify the multi-timescale nature of SMM. In this regard, λ and $K(\tau)$ are complementary in encoding the system's memory but they play distinct roles. The λ is the instantaneous (local-in-time) linear feedback term, which is also known as decay timescale in the context of classical reduced-order models used to characterize SMM timescale (e.g., Delworth and Manabe, 1988). It determines how quickly the state responds instantly to its previous state — providing a tool to capture system's fast memory timescale (τ_F), to be computed as below:

$$\tau_F = \frac{1}{|\lambda|} \tag{20}$$

Unlike λ, the $K(\tau)$ kernel captures the slow accumulation of memory across several lag steps. It weighs past values of θ_{root} and thus encodes how the older states still have a role to play in θ_{root} evolution. It can therefore be used to quantify the multiscale nature of slow memory of soil moisture. The shape and integral properties of $K(\tau)$ determine the extent and timescales of distributed memory (short-term, mid-term, long-term, etc.). In practice, one can plot cumulative memory-kernel for lags larger than 1 and explore the existing of slow-memory at different timescales in the system (Schmitt and Schulz, 2006). We differentiate between the various slow-memory timescales by isolating the memory accumulation behavior into several linear segments, each with a different memory accumulation rate (see, for example, Fig. 4 and 6). The memory accumulation at different segments is possibly controlled by different drivers, which are hypothesized in Table 1, and is addressed to some extent in Results and Discussion section but require detailed examination in future. When segmentation is done, the final lag value at each stage then provides the corresponding timescale. The number of identifiable segments depends on the resolution and length of the soil moisture data used, as well as the hydro-climatological conditions. With sufficiently longer time series, larger numbers are usually associated with high-resolution data (e.g., 5 segments for sub-daily sampling), while smaller numbers are associated with low-resolution data (e.g., 4 for daily sampling and 3 for monthly sampling). However, depending on the hydro-climatological or soil conditions, earlier memory accumulation stages might be unidentifiable even with high-resolution data, since the system undergoes a rapid transition from fast to slow memory accumulation. Conversely, if data is not monitored for long enough, the later stages of memory accumulation might be missed. A maximum of five linear segments can be identified, namely segments 1 to 5, which can also be referred to as stage I to stage V memory accumulation. These stages correspond to memory accumulations occurring at very short to long lags, respectively. Accordingly, five different slow-memory timescales, corresponding to each of these stages, are detectable. These will be referred to as the very-short-term slow-memory timescale (τ_{VSS}, corresponding to stage-I memory accumulation and only detectable at sub-daily sampling if hydro-climatological condition allows), the short-term slow-memory timescale (τ_{SS}, corresponding to stage-II memory accumulation and only detectable at daily or lower sampling upon favorable hydro-climatological condition), the mid-term slow-memory timescale (τ_{MS}, corresponding to stage-III memory accumulation), the long-term slow-memory timescale (τ_{LS}, corresponding to stage-IV memory accumulation), and the memory saturation timescale (τ_{SAT}, corresponding to stage-V memory accumulation). The latter stages (stage-III to stage-V) can be identified at all temporal resolutions in case the soil

https://doi.org/10.5194/egusphere-2026-549
Preprint. Discussion started: 4 February 2026

moisture time series used for this analysis is monitored over a sufficiently long period. This allows the system to accumulate memory at the longer lag steps.

Table 1- Possible physical mechanisms associated with LIDE-derived soil moisture memory timescales.

Memory timescale	Typical duration	Primary physical mechanisms	Interpretation§
Fast (τ_F) & vary-Short-term slow-memory (τ_{VSS})	Hours – days	•Bare-soil evaporation •Rapid canopy interception & evaporation •Shallow infiltration & redistribution •Topsoil hydraulic equilibration •Rapid transpiration sensitivity± •Daily weather persistence†	Controls initial decay of anomalies; Reflects fast surface–atmosphere coupling and shallow water turnover
and Short-term slow-memory (τ_{SS})	Days – months	•Root-zone water storage buffering •Mid-depth soil drainage •Early-season vegetation phenology •Short-term shallow groundwater influence •Seasonal PET changes	Represents root-zone mediated seasonal memory; System stores anomalies beyond synoptic timescales
Mid-term slow-memory (τ_{MS})	Months - seasons	•Seasonal recharge and depletion •Sub-root-zone infiltration pulses •Seasonal vegetation water-use memory •Soil thermal and PET seasonality •Intraseasonal moisture anomalies carryover	Governs season-to-season memory transfer; Enables reemergence-like behavior and sustained anomaly persistence
Long-term slow-memory (τ_{LS})	Season - years	•Deep vadose-zone storage and leakage •Groundwater–soil moisture feedback •Vegetation structural legacyς •Rare deep recharge events •Drought-induced ecosystem carryover	Describes interannual memory; Responsible for multi-year drought persistence and hydrologic legacy effects
Saturation memory (τ_{Sat})	Years - decades	•Deep drainageʒ •Long-term groundwater fluctuations •Soil structural evolutionՐ •Vegetation community shiftsՔ •Decadal climate modes (NAO, PDO) modulating moisture supply	Determines the outer envelope of SMM; The time it takes for cumulative memory to asymptotically saturate

§ Interpretation: what this memory timescale means for the soil–plant–atmosphere system
± Stomatal response
† Synoptic variability
ς Root-depth shifts and biomass changes
ʒ Fractured bedrock, deep sediments
Ր Freeze–thaw and shrink–swell
Ք Grass ↔ shrub transitions

https://doi.org/10.5194/egusphere-2026-549
Preprint. Discussion started: 4 February 2026

2.4. Automated Logit–Piecewise Memory Segmentation (LPMS) Method

To extract multiscale slow-memory characteristics from $K(\tau)$ kernel, we developed an automated Logit–Piecewise Memory Segmentation (LPMS) method. This method decomposes the cumulative memory kernel into physically interpretable segments/stages, as defined above (see Fig. 4 and 6). It involves fitting a parametric logit model, followed by piecewise linear segmentation in logarithmic lag space to detect distinct phases of memory accumulation and saturation. When soil moisture time series are sampled at frequencies of daily or longer (e.g. weekly or monthly), a single logit function, with or without one linear segment at very short lags, adequately explains the cumulative kernel. We refer to this behavior as unimodal memory accumulation. However, for soil moisture time series sampled more frequently (e.g. sub-daily—hourly), two logit functions are needed to fit the early- and late-time memory accumulation behaviors (see Fig. 6). We refer to this behavior as bimodal memory accumulation. In both cases, whether the memory accumulation behavior is unimodal or bimodal, LPMS uses the smoothed reference cumulative kernel curve obtained from logit fit to detect the linear segments. To do this, the LPMS method comprises several steps, which are described below:

Step 1: Preprocessing and Transformation

Given that $K(\tau)$ is the discrete memory kernel provided by LIDE and evaluated at integer lags, τ = 1, ..., N, where N is the length of the soil moisture time series, we first calculate the cumulative kernel $\mathcal{K}$ as follows:

$$\mathcal{K}(\tau) = \sum_{i=1}^{\tau} K(i) - K(1) \tag{21}$$

The $\mathcal{K}(\tau)$ [T^{-1}] defined as above represents the accumulated memory contribution up to lag τ. To linearize the asymptotic saturation behavior and stabilize the regression of long-lag dynamics, it is also necessary to transform the lag axis to logarithmic space:

$$t = \ln(\tau) \tag{22}$$

where t is dimensionless lag. We will, then, perform all subsequent fitting and segmentation in $(t, \mathcal{K})$ space.

Step 2: Fitting the Primary Logit Function (PLF)

The first step in the automated multiscale memory identification process involves fitting a four-parameter logit function to (t, $\mathcal{K}$), which enables us to capture the global sigmoidal shape of cumulative memory accumulation $\widehat{\mathcal{K}}$:

$$\widehat{\mathcal{K}}(\tau) = \alpha + \frac{\beta}{1 + exp\left(-\frac{t - \mu}{S}\right)} \tag{23}$$

where α is the lower asymptote [T^{-1}], β the amplitude [T^{-1}], and S and μ (both dimensionless) control slope and inflection location. The PLF fit is naturally dominated by the long lag part of the data, providing a smooth curve that can be used as a reference for identification of the transitions in memory accumulation regimes. When smoothed curve $\widehat{\mathcal{K}}(\tau)$ is obtained, the method then moves on to identify linear segments. However, as the identification of some segments (e.g., segments 4 and 5)

https://doi.org/10.5194/egusphere-2026-549
Preprint. Discussion started: 4 February 2026

is a prerequisite for the identification of others, the process will start with segments 4 and 5 identification rather than following them in order.

Step 3: Identification of the Active Memory Accumulation Regime (Segment 4, Stage-IV)

The active memory accumulation phase (Stage-IV) is designed around the inflection point of the PLF. To identify the best-fit line of the Stage-IV, the vertical midpoint of the PLF — with coordinate of $(t_{MP}, \hat{\mathcal{K}}_{MP})$ — is determined, where:

$$\hat{\mathcal{K}}_{MP} = \alpha + \frac{\beta}{2} \tag{24}$$

Accordingly, the corresponding lag t_{MP} is determined by minimizing $|\mathcal{K}(t) - \hat{\mathcal{K}}_{MP}|$. The local linear approximation is, then, formed using two neighboring points on $\hat{\mathcal{K}}(\tau)$ around t_{MP} (e.g., $y = [\hat{\mathcal{K}}(t_{MP} - 1), \hat{\mathcal{K}}(t_{MP}), \hat{\mathcal{K}}(t_{MP} + 1)]$ and $x = [t_{MP} - 1, t_{MP}, t_{MP} + 1]$), leading to a best-fit line defining the segment 4 and its accumulation rate, m_4:

$$\hat{\mathcal{K}}_4(t) = m_4 t + b_4 \tag{25}$$

The obtained best-fit line is valid for $t_{LB} < t < t_{UB}$, where t_{LB} defines the breakpoint lag value between rising tail of PLF and its lower plateau — with coordinate of $(t_{LB}, \hat{\mathcal{K}}_{LB})$ — and t_{UB} defines the breakpoint lag value between rising tail of PLF and its upper plateau — with coordinate of $(t_{UB}, \hat{\mathcal{K}}_{UB})$. The upper breakpoint $(t_{UB}, \hat{\mathcal{K}}_{UB})$ can be determined from the intersection of the upper PLF asymptote $\hat{\mathcal{K}} = \alpha + \beta$ and the best-fit line of segment 4, and the lower breakpoint $(t_{LB}, \hat{\mathcal{K}}_{LB})$ from the intersection of the lower PLF asymptote $\hat{\mathcal{K}} = \alpha$ and the best-fit line of segment 4. The obtained t_{UB} value defines the onset of the saturation plateau (segment 5 or stage-V memory accumulation), which will be identified in next step, and t_{LB} provides an upper limit for early-time segmentation and will be used to both detect the mid-term slow-memory accumulation regimes and, if needed, to condition the fit of a Secondary Logit Function (SLF) when high resolution data (e.g., sub-daily) is available.

Step 4: Identification of the Saturation Plateau (Segment 5, Stage-V)

To obtain best-fit line of segment 5 and its accumulation rate, m_5, a linear regression is performed over $(t, \hat{\mathcal{K}})$ for all datapoints beyond the onset of the saturation plateau with $t > t_{UB}$, leading to:

$$\hat{\mathcal{K}}_5(t) = m_5 t + b_5, \qquad \text{where} \qquad t > t_{UB} \tag{26}$$

Step 5: Early-Time Memory Regimes Identification (Segments 1-3)

Depending on the number of segments prescribed (n_segments = 3, 4, or 5), we resolve the early-time behavior as follows whereas only one of the options given will be followed:

a) Three-segment configuration (Segment 3 only)

With n_segments set to 3, only segments 3 to 5 are detectable. Having already detected segments 4 and 5 in previous steps, this step only requires the identification of segment 3, with segments 1 and 2 remaining undetectable under this configuration.

https://doi.org/10.5194/egusphere-2026-549
Preprint. Discussion started: 4 February 2026

In this case, the memory accumulation through all lags smaller than t_{LB} is approximated by a single slow-memory accumulation line (namely, segment 3, stage-III), with a linear regression model constraint with fixed intercept value of $\mathcal{K}(1)$:

$$\hat{\mathcal{K}}_3(t) = m_3 t + \mathcal{K}(1), \quad \text{where} \quad t < t_{LB} \tag{27}$$

where m_3 defines the memory accumulation rate for the third segment.

b) Four-segment configuration (segments 2 and 3)

With n_segments set to 4, only segment 1 remains undetectable. Therefore, the memory accumulation through lags smaller than t_{LB} requires to be approximated by two slow-memory accumulation lines (namely, segments 2 and 3; memory accumulation stage-II and stage-III). For this aim, to determine the transition from stage-II to stage-III, a sequential linear approximation method is applied to identify a critical lag t_{crit} by scanning forward from the origin until a goodness-of-fit threshold (e.g., a correlation coefficient, R^2, value of 0.8) is violated. Then, the best-fit line of segment 2 is obtained by a linear regression over $(t, \mathcal{K})$ for all datapoints conditioned by $t < t_{\text{crit}}$:

$$\hat{\mathcal{K}}_2(t) = m_2 t + b_2, \quad \text{where} \quad t < t_{\text{crit}} \tag{28}$$

where m_2 defines the memory accumulation rate for second segment.

Similarly, fitting a second linear regression over $(t, \hat{\mathcal{K}})$ for all datapoints with $t > t_{\text{crit}}$ and $t < t_{LB}$ will lead to best-fit line for segment 3. However, here we fix the intercept to $\hat{\mathcal{K}} = \alpha$ to enforce consistency with the global shape of the cumulative memory kernel:

$$\hat{\mathcal{K}}_3(t) = m_3 t + \alpha, \quad \text{where} \quad t_{\text{crit}} < t < t_{LB} \tag{29}$$

where m_3 defines the memory accumulation rate for the third segment.

c) Five-segment configuration (segments 1 to 3)

To resolve the very-short-term (stage-I memory accumulation) and short-term (stage-II) regimes (only possible with high resolution data), we fitted an additional logit function (namely, SLF) to the early lag subset of the cumulative memory kernel: $(t, \mathcal{K})$, for all data points with $t < t_{LB}$. For this range, the SLF therefore replaces the PLF. Under this configuration, the best-fit line of segment 2 is obtained from a local linearization around the midpoint of the SLF, using the same procedure as in step 3. This leads to the following regression, where m_2 is the memory accumulation rate for the second segment:

$$\hat{\mathcal{K}}_2(t) = m_2 t + b_2 \tag{30}$$

The best-fit line of segment 1 is identified by the same sequential linear approximation method applied in previous stage, leading to:

$$\hat{\mathcal{K}}_1(t) = m_1 t + b_1, \quad \text{where} \quad t < t_{\text{crit}} \tag{31}$$

where m_1 defines the memory accumulation rate for the first segment. Finally, the best-fit line of segment 3 is derived from a linear fit to datapoint falling between 90 % upper quantile of SLF values and t_{LB}, leading to:

$$\hat{\mathcal{K}}_3(t) = m_3 t + \alpha \tag{32}$$

https://doi.org/10.5194/egusphere-2026-549
Preprint. Discussion started: 4 February 2026

where m_3 defines the memory accumulation rate for the third segment. The ideal number of n_segments should be determined by first running the analysis at optional value, plotting the results and then performing a secondary analysis with the optimum visible segments chosen.

Step 6: Saturation Plateau Spread and Reemergence Features

Seasonal periodic oscillations in the saturation plateau are detected via peak–valley analysis using 'find_peaks' algorithm with a physically motivated high distance (365 days for daily data, 12 for monthly, etc.). Linear fits to the upper and lower envelopes return reemergence amplitude and spread; while intersect of envelopes provides a reemergence-related (empirical) timescale for saturation (Kumar et al., 2019).

Step 7: Quantification of Characteristic Timescales

Finally, by completing the segmentation process, the following memory timescales are extracted:

- Fast memory timescale (τ_F) based on inversion of λ.
- Very-short-term (τ_{VSS}), short-term (τ_{SS}), mid-term (τ_{MS}), and long-term (τ_{LS}) slow memory timescales being determined by intersecting successive linear segments. For example, the intersection of segment 1 and segment 2 determines τ_{VSS}, and so on.
- Saturation timescale (τ_{Sat}): the lag at which upper and lower envelopes of saturation plateau meet.
- Quantile-based timescales: lags at which $\widehat{\mathcal{K}}(t)$ reaches 10%, 50%, and 90% of its saturation level, defined as τ_{10}, τ_{50}, and τ_{90}.

All lag-domain timescales are converted to physical units with the given temporal resolution (either days, hours, or months). When high-resolution data (e.g. hourly) is available, the τ_F usually operates at sub-daily scales (e.g. hours to several hours), the τ_{VSS} at sub-daily to daily scales (e.g. several hours to several days), the τ_{SS} at daily to monthly scales, the τ_{MS} at monthly to seasonal scales, the τ_{LS} at seasonal to yearly scales and the τ_{Sat} at yearly to decadal scales. Such clear differentiation between scales supports the idea that different combinations of drivers control each SMM timescale, a topic that will be elaborated on in the Results and Discussion section (see Table 1). However, it is worth noting that when the data examined is too coarse (e.g., daily or monthly) to identify earlier timescales (e.g. τ_{VSS} or τ_{SS}), then the timescale captured by τ_F will be an integration of those unidentified timescales. Consequently, larger fast memory timescales (e.g. up to several days for daily data and up to several months for monthly data) may be observed at larger temporal resolutions.

3. Materials and Methods

3.1. Study Sites and Data

The data utilized in this paper to demonstrate the application of the developed LIDE framework in examining the dynamics of θ_{root} as well as analyzing its memory effects were collected using a set of weighable, high-precision grassland lysimeters — with a cross-sectional area of 1 squared-meter and a depth of 1.5 meters — installed at experimental field sites, including six

https://doi.org/10.5194/egusphere-2026-549
Preprint. Discussion started: 4 February 2026

lysimeters at the energy-limited site in Rollesbroich (50°37′12”N, 6°18′15”E) and three lysimeters at the water-limited site in Selhausen (50°52′7′′N, 6°26′58′′E) (Bogena et al., 2018; Pütz et al., 2016; Rahmati et al., 2020). Both experimental sites are part of the TERENO-SOILCan lysimeter networks in Germany located in Eifel/Lower Rhine Valley Observatory of TERENO in Germany (Bogena et al., 2018; Pütz et al., 2016). We used the six-year (2013-2018, i.e. 2191 days) preprocessed time series data provided by Rahmati et al. (2020), and interested parties may refer to that paper for more information on data collection, preprocessing, and cleaning steps. Briefly, all lysimeters are equipped with time-domain reflectometry (TDR) probes (CS610 and TDR100, Campbell Scientific, North Logan, UT, USA) to measure soil water content at three different depths (10, 30, and 50 cm) at 30-minute intervals.

In addition to data from above lysimeters sets, we also used data from cosmic-ray neutron sensors (CRNSs) in Schöneseiffen station (50°30'53.6"N 6°22'32.1"E), as part of COSMOS-Europe dataset (Bogena et al., 2022), which meteorologically is acting in between energy-limited site of Rollesbroich and water-limited site of Selhausen, and therefore, we call it as intermediate site in the context of this analysis. The station is equipped with three sets of sensors, each set acting as one replicate and therefore, in this analysis we used an average of those three replicates as representative soil moisture data of the station. Furthermore, each replicate consists of three different sensors installed at three different depths of 5, 20, and 50 cm.

3.2. Soil profile configuration

To apply the LIDE framework and its helper model of LPMS, root-zone soil moisture, θ_{root}, data was required. In this regard, we used high-quality soil moisture data collected from our lysimeters in Rollesbroich and Selhausen, and from the CRNS station in Schöneseiffen, as mentioned above. Since a detailed root zone characterization was not available, we simply averaged the aforementioned depth-wise observations to obtain the θ_{root} data required for this analysis. We are aware that such an average value might not represent the θ_{root} perfectly, but it still provides a good proxy for that. It is worth noting that the maximum rooting depth reported for the analyzed sites is 127–135 cm (Boden, 2005).

3.3. LIDE and LPMS Application

To obtain the parameters of the LIDE framework — i.e. λ, $K(\tau)$ and $F(t)$, we used the numerical solution introduced in subsection 2.2, together with six years' (2013–2018) θ_{root} data, as described in the previous subsection. Having obtained the memory-related components — i.e. λ and $K(\tau)$, we applied, then, the LPMS method (see subsection 2.4) to detect several SMM timescales, as discussed previously.

The θ_{root} data had a daily temporal resolution for the energy-limited Rollesbroich site and the water-limited Selhausen site. Therefore, we applied the numerical solution to both the daily and monthly resampled data from Rollesbroich and Selhausen. However, the θ_{root} data at the intermediate Schöneseiffen site is provided at a half-hourly resolution, so we first resampled the data into hourly, daily and monthly resolutions, and then applied the LIDE framework to each series separately. This enabled us to evaluate the applicability of the LIDE model to the θ_{root} data at different temporal resolutions (i.e. hourly, daily and monthly).

https://doi.org/10.5194/egusphere-2026-549
Preprint. Discussion started: 4 February 2026

Regarding the LPSM method, one requirement is to determine the optimal number of linear segments observable on the cumulative memory kernel curve. Our first run of the LPSM method revealed that five, four and three linear segments were identifiable when hourly, daily and monthly data were analyzed for Schöneseiffen, which acts as an intermediate site for hydrometeorological conditions. Similarly, four and three linear segments were identifiable when the LPSM method was applied to the LIDE-driven memory kernel from the energy-limited Rollesbroich site. However, at the water-limited Selhausen site, three linear segments were identifiable for both daily and monthly resolutions, which is a good example of how the hydrometeorological conditions can affect the memory kernel segmentation, which is elaborated on in the Results and Discussion section.

3.4. Additional Logit-based Memory Characteristics Obtained from LPMS method

Although, the logit function fitted in LMPS method is mainly used to smooth the cumulative memory kernel simplifying linear segmentation procedure, at the meantime it also provides parameters that can be used for memory characteristics quantification: with α as baseline cumulative memory [T^{-1}], $\alpha + \beta$ as total memory capacity [T^{-1}], μ as characteristic memory lag [-], and S as active memory spread [-]. Therefore, we used these parameters to explore the global memory embedded in data. In this regard, we calculated the total capacity $\widehat{\mathcal{K}}_C = \alpha + \beta$ and half-capacity timescale $\tau_{50} = e^{\mu}$ using obtained logit parameters. On the other hand, physically, the α parameter of logistic function corresponds to the residual fast memory or any offset in cumulative memory before distributed memory processes start accumulating. In theory, since fast memory — $K(\tau = 1)$ — is excluded, one might expect an α-value of zero. Therefore, we use any deviation of α parameter from zero as a residual fast memory quantifier, r_F. Parameter β determines the total amplitude of memory accumulation being equal to the difference between the lower and upper asymptotes of the logistic curve. The sum of α and β can be used to determine the saturated cumulative memory kernel, i.e. the total integrated influence of past soil moisture states ($\widehat{\mathcal{K}}_C = \alpha + \beta$). Hereafter, this is referred to as memory capacity, $\widehat{\mathcal{K}}_C$. In general, larger β values indicate greater total system memory capacity, meaning the soil–plant–atmosphere system retains a stronger influence from past moisture anomalies, so it is logical to use it to quantify SMM capacity (as an indicator of memory strength) on top of the SMM timescales. Comparing $\widehat{\mathcal{K}}_C$ across different hydro-climate sites can provide a quantitative measure of relative memory capacity between climates or soil types. The characteristic memory lag, μ, is the lag at which the rate of memory accumulation is maximal, which corresponds to the midpoint of the S-shaped curve (e.g., inflection point of the logistic function). Therefore, we interpret it as the dominant or central timescale of slow-memory processes, which, in a sense, play the role of the 'half-life' of memory build-up, when α is zero. In general, the smaller μ, the faster the system reaches memory saturation (it saturates quickly); a larger μ leads to a slower increase and longer persistence. In the same sense, S controls the slope or spread of the logistic curve around the inflection point. From physical perspective, a smaller S means sharp transition from fast-memory to slow-memory saturation (i.e., highly organized, narrow-band memory response) and short active period of memory while a larger S means gradual transition which can lead to diffuse and multi-timescale persistence. From hydrological perspective, S quantifies how distributed the slow memory is.

https://doi.org/10.5194/egusphere-2026-549
Preprint. Discussion started: 4 February 2026

Smaller S values can indicate to well-buffered systems (fast turnover), while larger S values indicate long retention and heterogeneous storage pathways in the system.

Additionally, the memory capacity, $\widehat{\mathcal{K}}_c$, either can be determined by summing up α and β parameters of logit function — which we call it as estimated memory capacity— or by determining the coordinates of actual memory saturation point by intersecting the upper and lower envelopes of saturation phases oscillations, which we call it as actual memory capacity, noted by $\mathcal{K}_C$. Then, we also use the difference between estimated and actual memory capacity to quantify residual slow-memory of the system, r_S, as below:

$$r_S = \frac{\mathcal{K}_C - \widehat{\mathcal{K}}_C}{\mathcal{K}_C} \times 100 \tag{33}$$

4. Results and Discussion

4.1. Soil moisture dynamics at examined sites

Inspecting the observed θ_{root} signals at energy- and water-limited sites (Fig. 2) reveals a considerable and almost identical decreasing trend (with a slope of 0.9 ± 0.1 percent per year; Fig. 2-b) from 2013 to 2018. This indicates a widespread drying signal across both regimes, with the intermediate site showing no clear trend (excluding from Fig. 2). One plausible proximate driver of the concurrent drying at both sites seems to be an increase in evaporative demand, and/or reductions in effective precipitation over the observation period, which is also reported at European scale for the recent decades (Bevacqua et al., 2024; Gao et al., 2014; Rahmati, Graf, et al., 2023).

The distinguishing behavior of the summer minimum θ_{root} values in examined regimes (Fig. 2-c) indicates different mechanisms of the limiting effect at each site. For the energy-limited site, the yearly minimum value is strongly decreased and revealed a negative trend; ≈-18 % lower in 2018 than in 2013. This suggests that the factors that normally limit evapotranspiration in wet years are gradually weakening, e.g., the increase in atmospheric demand makes the atmosphere able to draw more water from the root-zone when it is available. On the other hand, the water-limited site's minimum shows a barely reduced variation. This can be explained by the idea of a hydrological "floor": as the soils are situated near the minimal extractable water or the plant stomata close in strong water stress, there is little effect that a further increase in the atmospheric demand can exert to θ_{root}. Such asymptotic behavior near the residual or plant-available water threshold is a common pattern for water-limited systems (Liu et al., 2024). Again, the intermediate site showed no clear trend for summer minimum θ_{root} values as well.

The observed drying signal has implications for SMM and soil moisture persistence, with two points worth highlighting as context: First, the reduction in mean θ_{root} and the lowering of summer minimum at the energy-limited site will likely change the system's memory timescales since memory depends on both storage magnitude and the partitioning of water fluxes. In particular, the reduction in shallower or drier stores can decrease the persistence of anomaly on a seasonal time scale, but deepened root-zone storage and vegetation buffering is known to increase multi-month memory (Rahmati et al., 2024). Thus, drying can lengthen or shorten characteristic memory depending on the process that is most changed. Second, the near-constant

https://doi.org/10.5194/egusphere-2026-549
Preprint. Discussion started: 4 February 2026

floor in the water-limited site suggests that below a certain threshold, the system's response to perturbations becomes non-linear. Hence, this is limited by residual moisture and external stomatal or climatic feedback, and it directly impacts memory metrics based on anomaly decay rates and autocorrelation. These mechanistic hypotheses will drive the SMM assessment, being presented as follows.

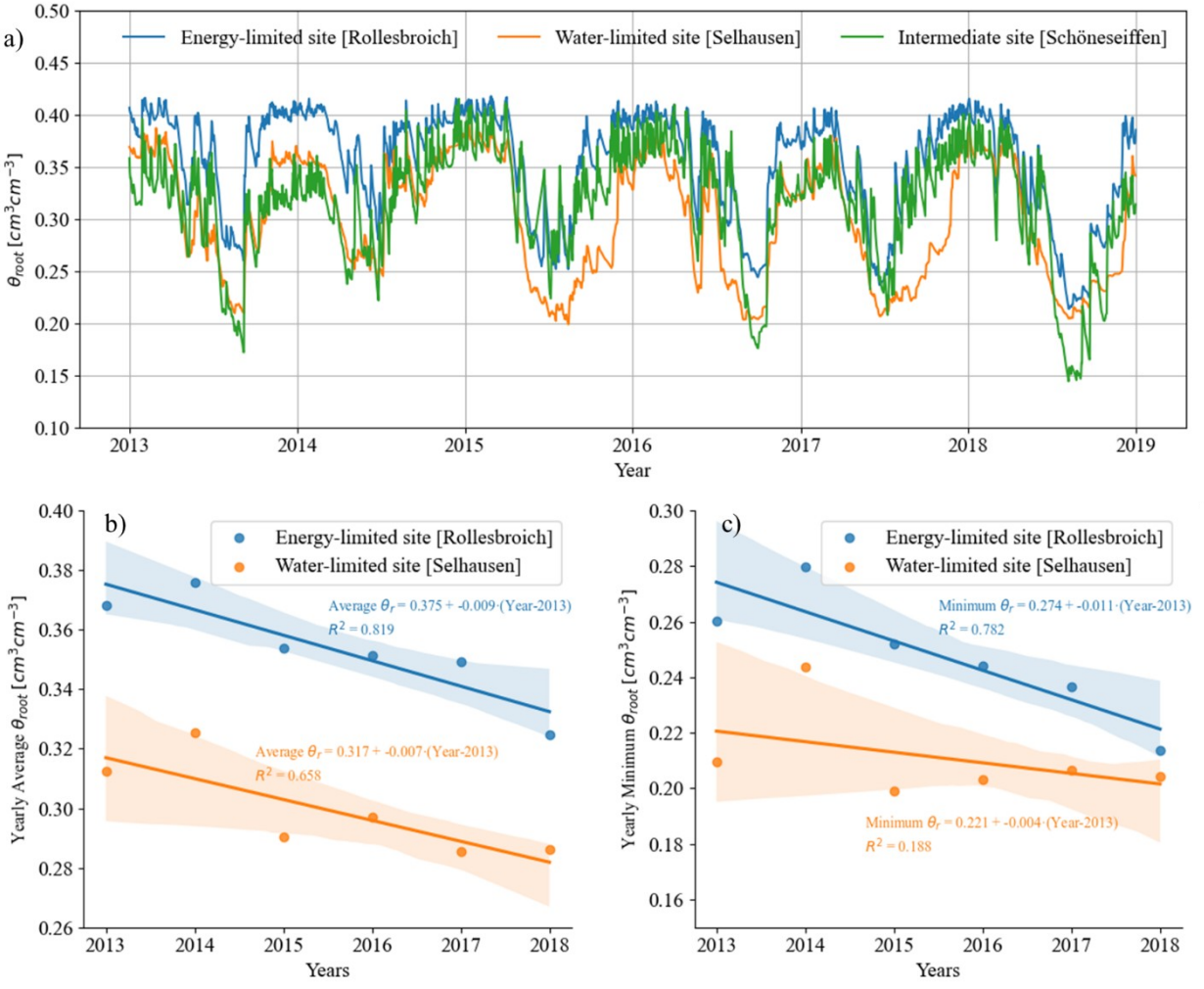

Figure 2 -Variation of root zone soil moisture (θ_{root}) at energy-limited, water-limited, intermediate sites. a) Time series of daily θ_{root}, b) yearly average of θ_{root}, and c) minimum value recorded in summer times.

4.2. Multiscale soil moisture memory characterization over daily data

We solved the LIDE model numerically according to Schmitt and Schulz (2006) based on daily measured θ_{root} values and thereby determined the λ, $K(\tau)$, and $F(t)$ parameters (see Fig. 3), and consequently identified the multi-timescale nature of SMM through application of automated LPMS method. The variation of cumulative memory kernel $\mathcal{K}(\tau)$ for the examined sites are presented in Fig. 4. A careful examination of $\mathcal{K}(\tau)$-curves reveals four distinct stages (Fig. 4): (i) a stage-II early

https://doi.org/10.5194/egusphere-2026-549
Preprint. Discussion started: 4 February 2026

slow-memory accumulation at short to intermediate lags (days-months), (ii) a stage-III intermediate slow-memory accumulation at intermediate to long lags (months-seasons), (iii) a stage-IV active late slow-memory accumulation (seasons-years), and finally (iv) a near-flat tail (stage-V) for long lags (years-decades). Through this, the LIDE-derived memory spectrum decomposes SMM in physically meaningful timescales that are dominated by specific hydrological and ecohydrological processes. As mentioned previously, the very-early slow-memory accumulation stage (namely, stage-I), which usually operates at hours to days scale is not identifiable by daily moisture data.

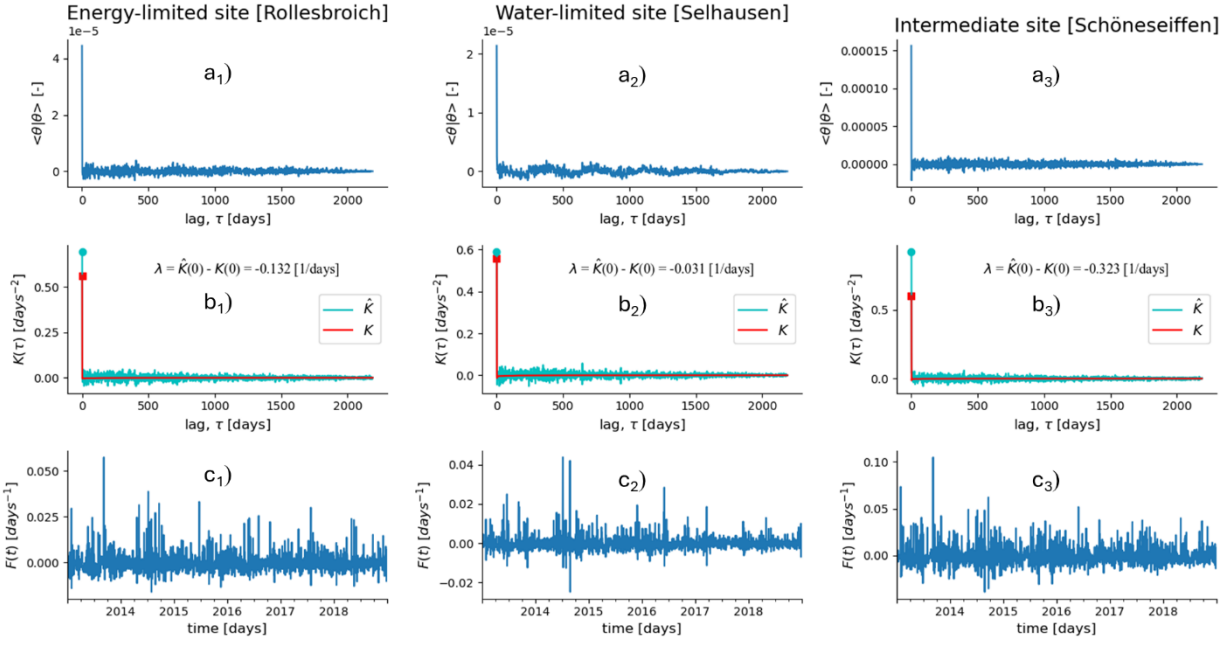

Figure 3 – The variation of LIDE framework parameters over time or lag domains, obtained from daily root-zone soil moisture (θ_{root}) signals at energy-limited (subscript 1), water-limited (subscript 2), and intermediate (subscript 3) sites. a) Autocorrelation function, $\langle\boldsymbol{\theta}|\boldsymbol{\theta}\rangle$, b) memory kernels $\boldsymbol{K(\tau)}$ and $\widehat{\boldsymbol{K}}(\boldsymbol{\tau})$, and c) noise term $\boldsymbol{F(t)}$

https://doi.org/10.5194/egusphere-2026-549
Preprint. Discussion started: 4 February 2026

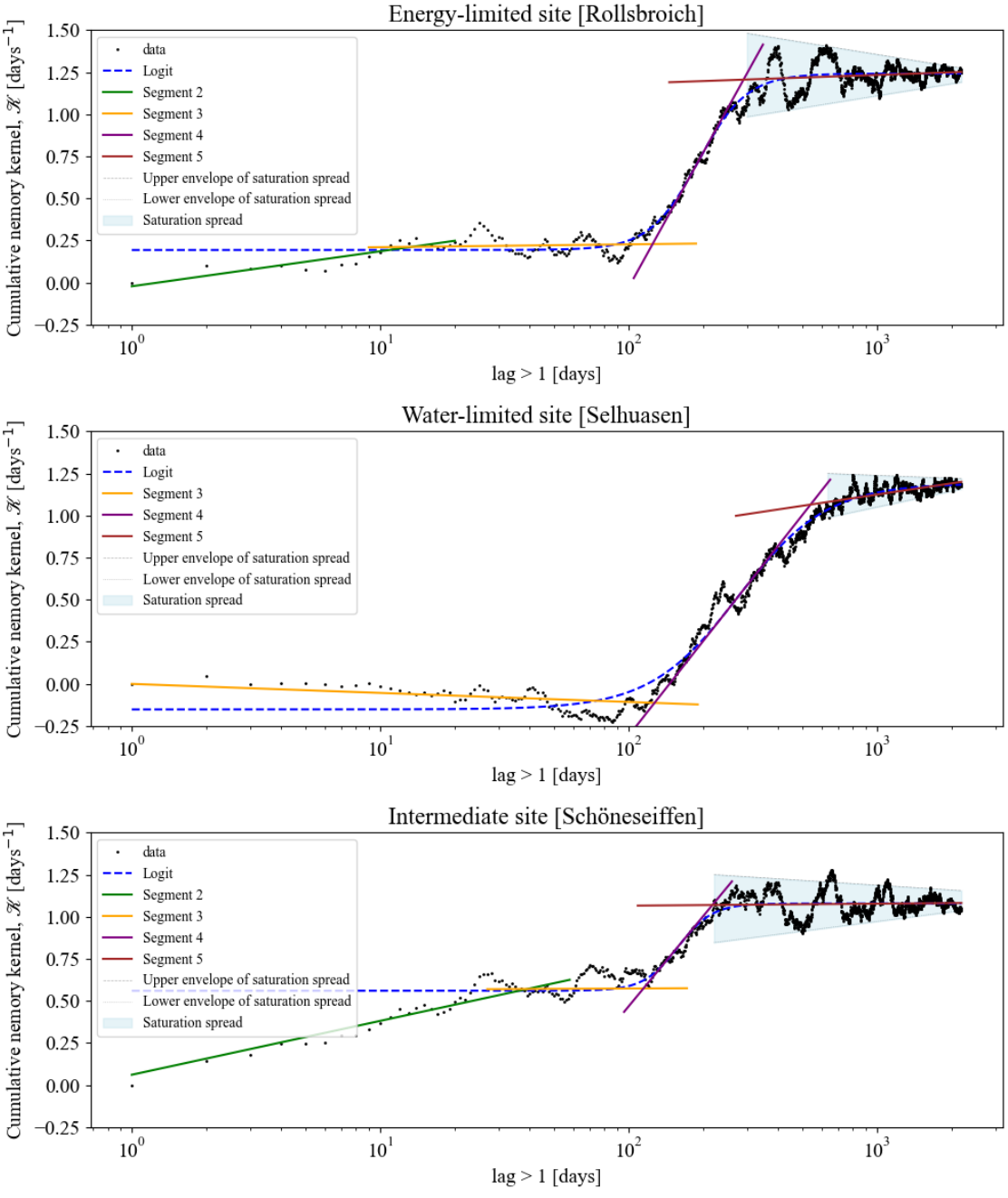

Figure 4 – Cumulative memory kernel $\mathcal{K}(\tau)$ for energy-limited (Rollesbroich; top panel), water-limited (Selhausen; middle panel), and intermediate (Schöneseiffen; lower panel) sites, demonstrating increasing cumulative distributed-soil-moisture memory with lag ($\tau > 1$ days). According to memory accumulation, four distinct stages are recognized: Stage-II (early slow-memory accumulation), Stage-III (intermediate slow-memory accumulation), Stage-IV (active late slow-memory accumulation), and Stage-V (attainment of the memory saturation). Intersection points between each two consecutive stages indicate switching between stages, consequently corresponding timescale. The saturation spread is shown as a shaded envelope.

https://doi.org/10.5194/egusphere-2026-549
Preprint. Discussion started: 4 February 2026

4.2.1. Fast memory of soil moisture

For the daily resolved data used in our analysis, the fast memory timescale ($\tau_F = 1/|\lambda|$, describing how the system responds immediately to perturbations—usually in timescales of days–weeks/months) is the first identified memory timescale which we postulate it representing the effects of rapid near-surface–atmosphere exchange (see Table 1), including daily weather persistence (Koster et al., 2009), capillary redistribution (early-stage infiltration)(Morbidelli et al., 2011), shallow root water uptake adjustments (e.g., short-term vegetation water consumption)(Calabritto et al., 2024), and residual drainage (Aldrees and Nachabe, 2019) — the long tail of drainage occurring for some days after the occurrence of fast drainage at sub-daily timescale right after precipitation events — or evaporation from bare soil (Han and Zhou, 2013; Iden et al., 2021; Or et al., 2013) and topsoil hydraulic equilibration (Lehmann and Or, 2024). Considering the e-folding convention of Delworth and Manabe (1988), obtained τ_F values of ~7.6 days at the energy-limited site (see Table 2) imply that it only takes around one week for energy-limited site to reduce its initial perturbation to its e-folding — e.g., $\theta_{\mathrm{root}}(\tau_F)/\theta_{\mathrm{root}}(t_0) = e^{\lambda\tau_F} = e^{-1} \approx 0.37$; meaning that ~63% of the initial perturbation is dissipated after around one week. While it takes around four weeks for the water-limited site (with τ_F values of ~32.3 days) and around half week for intermediate site (with τ_F values of ~3.1 days). The substantially shorter fast memory at intermediate (≈3.1 days) and energy-limited site (≈7.6 days) sites where water is available sufficiently suggests relatively rapid dampening of soil moisture anomalies in those sites due to efficient wet-dry short-term surface flux exchanges (Koster et al., 2012; McColl, Alemohammad, et al., 2017; Orth and Seneviratne, 2013). In such moist environments, the evaporative response to available energy becomes strong even with relatively small increases in wet-energy availability, which drives rapid decay of anomalies (Miralles et al., 2011; Teuling et al., 2009). Conversely, the weaker instantaneous damping (≈32 days) at the water-limited site corresponds to the poor ability of this system to quickly remove anomalies, given that low soil moisture blocks evaporative fluxes with no regard for energy availability. Therefore, perturbations are sustained for longer periods of time before being modulated by slower, distributed processes captured in the memory kernel.

4.2.2. Slow-memory of soil moisture

In addition to τ_F, the LIDE framework decomposes the captured slow memory into three timescales (excluding the very-short-term slow-memory timescale, τ_{VSS}, which cannot be identified using daily data and will be addressed later when dealing with hourly data). These timescales are:

1) **Short-term slow-memory timescale (τ_{SS}):** captured by the stage-II early slow-memory accumulation at days to months timescales (occurring at lower rates of $+0.115 \pm 0.03$ day^{-1}; see Table 2) which likely reflects the near-surface processes (see Table 1) like stage-II evapotranspiration (Ghannam et al., 2016; Jacobs et al., 2020; McColl, Alemohammad, et al., 2017; McColl et al., 2019; McColl, Wang, et al., 2017; Seneviratne and Koster, 2012), gravity-induced water redistribution (late-stage infiltration)(Farmani et al., 2025), and root water uptake adjustments (Amenu et al., 2005; Thomas et al., 2009) which are mainly moderated by the soil's physical characteristics and vegetation activity (e.g., early-season vegetation phenology)(Cleverly et al., 2016; Rahmati et al., 2024). Probably, one can also

https://doi.org/10.5194/egusphere-2026-549
Preprint. Discussion started: 4 February 2026

expect the short-term groundwater influences especially at sites where water table is shallow (Martínez-de la Torre and Miguez-Macho, 2019). In addition, seasonal potential evapotranspiration changes (Stahl and McColl, 2022) also can have some effects on memory accumulation at this stage.

2) **Mid-term slow-memory timescale (τ_{MS})**: captured by Stage-III intermediate slow-memory accumulation, which occurs at slightly lower rates of +0.005 ± 0.002 day^{-1} at energy-limited and intermediate sites compared to slightly stronger but negative rate of −0.023 day^{-1} at water-limited site (see Table 2). We postulate that it picks up seasonal storage/recharge pulses and deeper transport processes (Stacke and Hagemann, 2016), whereby deeper groundwater can recharge the soil and sustain anomalies (Mu et al., 2021).

3) **Long-term slow-memory timescale (τ_{LS})**: captured by Stage-IV late slow-memory accumulation, occurring with relatively higher rates of 1.16, 0.814, and 0.775 days^{-1} in energy-limited, water-limited, and intermediate sites, respectively (see Table 2). We hypothesize that it results from storage in the deep vadose-zone, groundwater feedback and ecohydrological legacies (Gómez et al., 2022; Kaisermann et al., 2017; Müller and Bahn, 2022; Van Loon et al., 2024; Wang et al., 2024).

The most important insight learned from slow-memory timescale identification, probably, is that no τ_{SS} was identifiable at the water-limited site (Selhausen), while a τ_{SS} ~39 and ~13 days were detected at the energy-limited and intermediate sites, respectively (see Table 2 and Fig. 4). This is physically consistent with the hydroclimatic setting, whereby high evaporative demand, rapid post-rainfall drying, and shallow root-zone depletion (Laio et al., 2001; McColl et al., 2019; McColl, Wang, et al., 2017; Rahmati, Graf, et al., 2023) prevent short-lag anomalies from persisting and forming a coherent accumulation segment. Consequently, the system moves directly from fast memory to intermediate slow-memory behavior whereas deeper storage processes control persistence. The suppression of memory for short lags in drier regions has also been extensively documented (Ghannam et al., 2016; McColl et al., 2019). Furthermore, water-limited ecosystems are generally characterized by “concave-up” autocorrelation properties, i.e., memory falls at short lags but reappears at deeper/larger storage timescales (Kumar et al., 2019).

A positive Stage-II slow-memory accumulation slope would imply that both near-surface redistribution and rapid recharge contribute constructively to the total memory at the first finite few lags. Physically, such positive memory accumulation can occur when shallow recharge/near surface storage leads to a delayed re-supply that adds soil moisture change at later times – – for example, the effect of a wet day becomes "observable" again after few days once rainfall induced lateral redistribution and capillary rise had an impact. Such quick buffering and rapid redistribution often are in effect under moist conditions (i.e., energy-limited systems) and may generate a net positive weight for the short-lag kernel.

All examined sites are associated with a similar typical τ_{MS} values of 115–127 days (Table 2), suggesting a common seasonal period of sub-root and seasonal recharge activity. The rate of the mid-term accumulation is, however, different: positive at energy-limited (Rollesbroich; +0.007 days^{-1};) and intermediate (Schöneseiffen; +0.003 days^{-1}) sites and negative at water-limited site (−0.023 days^{-1}). This translates physically to a mechanism through which seasonal recharge and slow redistribution at Rollesbroich and Schöneseiffen reinforce SMM incrementally in the 3–4-month window; while, at Selhausen intermediate-

https://doi.org/10.5194/egusphere-2026-549
Preprint. Discussion started: 4 February 2026

lag processes would tend to damp down later moisture anomalies, $d\theta/dt$. Physically, such a dampening or delayed negative feedback could possibly result from: i) antecedent wetness leading to decreased subsequent infiltration (and surface runoff, and recharge)(Knapp et al., 2025; Song and Wang, 2019; Zhang et al., 2011) which is then reduces later recharge and related $d\theta/dt$; ii) plant physiological responses (stomatal control) leading to the lagged increase of water extraction (and consequently reducing current state of soil moisture) following a wet pulse (Buckley, 2019; Guo and Ogle, 2019; Thayamkottu et al., 2025); or iii) rapid post-rain redistribution taking water away from the root-zone (Li et al., 2025; Orozco-López et al., 2018; Pales et al., 2018) giving an intermediate-lag apparent negative kernel. For example, in the water-limited site, individual wetting and drying paths (hysteresis) would not necessarily coincide (Abdoli et al., 2024) which could mean that preferential or rapid flow pathways could divert infiltration away from the root-zone immediately after rain (Kargas et al., 2021; Nimmo et al., 2025; Zhang et al., 2018), leading to an intermediate negative contribution at intermediate positive lags.

Examined sites also demonstrate distinct behavioral differences according to the active Stage-IV memory accumulation and its associated memory timescale, τ_{LS}. The energy-limited site (accumulating memory at a time lag of 125–291 days) and intermediate site (at a time lag of 115–218 days) gain memory in a narrow time window. In contrast, it is widespread (accumulating memory at a time lag of 127–541 days) in the water-limited system. This combination indicates that the energy-limited and intermediate sites accumulate slow-memory quickly (within a seasonal band alone — perhaps through repeated seasonal recharge, efficient root-zone refilling, and tighter coupling between vegetation and soil storage), implying good seasonal persistence and therefore high sub-seasonal predictability. In contrast, the water-limited site integrates memory more slowly, but over a much longer temporal window, which is consistent with infrequent recharge events and deeper or decoupled storage and long hydraulic or vegetation lags that spread memory over longer time horizons to yield weaker per-day persistence at some ranges of lag but stronger tails from legacy effects. This contrasting behavior will have some implications from a hydro-climate perspective. For instance, the energy-limited regimes are likely to exhibit more pronounced sub-seasonal/seasonal predictability due to relatively concentrated memory (relevant for predictions on seasonal timescales), while water-limited regimes may exhibit longer extended, but weaker, predictability as information is spread out over larger lags. This is consistent with findings showing that land-atmosphere coupling and recharge dynamics regulate predictability and seasonal skill (Seo et al., 2024). In contrast, the energy-limited sites can also respond (and hence recover) quickly (but would also lose memory more readily when conditions change), and the processes at a water-limited site might be able to maintain a hydrological memory of extremes for longer time periods, potentially extending such legacy effects of drought compromising both vulnerability and recovery of the system (Rahmati et al., 2024).

4.3. Memory saturation, capacity, and reemergence

Besides the trinary slow-memory timescales identified as above, additional LIDE-induced insights about the examined hydro-climate regimes can be obtained: time to memory saturation, known as saturation timescale, τ_{Sat}, and memory strength captured by memory capacity, $\mathcal{K}_C$. Memory saturation represents the final stage of the memory accumulation (namely, stage-V) that evolves slowly and eventually approaches a saturation plateau, the memory capacity of $\mathcal{K}_C$, where past states do not

https://doi.org/10.5194/egusphere-2026-549
Preprint. Discussion started: 4 February 2026

play role any more in soil moisture evolution, which is mainly overlooked in classical SMM analysis. Physically this regime is associated with deep storage (Kollet and Maxwell, 2008), groundwater coupling (Irvine et al., 2024; Martínez-de la Torre and Miguez-Macho, 2019; Miguez-Macho and Fan, 2012), vegetation structure transformation, inter-annual carry-over of soil moisture anomalies (Kumar et al., 2019), or slow hydrological recovery and decadal climate variation (Seneviratne et al., 2010) (Table 1).

The energy-limited and intermediate sites have small residual saturation slopes of approximately 0.022 and 0.005 days^{-1} with a saturation window ranging beyond lag values of 291 and 218 days, respectively, whereas the water-limited site is associated with a larger residual slope of approximately 0.097 days^{-1} and a broader saturation window of beyond 541 days. The slightly positive finite lag momentum at the energy-limited and intermediate sites suggests that the system is essentially finite lag saturated, i.e. any additional memory gained at very long lags comes with only a small premium in terms of per-day memory and is accumulated slowly over multi-year time spans. Conversely, the much higher slope at the water-limited site suggests that long-lag memory accumulation is ongoing. Probably, deep storage buffering, infrequent yet significant recharge events, and gradual vegetation and soil adjustments generate noticeable legacies that accumulate over time. The residual slow-memory fraction calculation (see Table 2) reveals an r_S values of ~0.7%, ~3.5%, and ~1.5% at energy-limited, intermediate, and water-limited sites, respectively. Assuming a residual memory fraction of less than 1% as practical importance threshold, the energy-limited site is already saturated, the water-limited site is very close to saturation, whereas the intermediate site still is very far from saturation and due to lower rate of memory accumulation at saturation plateau, gaining a full saturation will be time-consuming whereas theoretically the full memory saturation (quantified as τ_{Sat}) occurs after around nine years in energy- and water-limited sites while it will take around 15 years for intermediate site. Hydrologically, this means that knowledge of the previous state beyond τ_{LS} at the energy-limited and intermediate sites makes very limited improvement to seasonal forecasting, while the water-limited site retains some useful long-lead memory and is probably somewhat more susceptible to multiyear drought legacies.

The asymptotic memory capacity ($\mathcal{K}_C$) obtained (see Table 2) is similar between sites (1.18 ± 0.05 days^{-1}) with slightly being slower in intermediate site (with $\mathcal{K}_C$ = 1.12 days^{-1}), indicating a similar total storage potential but different partitioning among timescales. As a result, in energy-limited conditions, there is rapid accumulation of memory and strong short-term predictability while water-limited conditions spread memory over wider lags, providing weaker short-term persistence but stronger long-term legacy. In the intermediate site, possibly where both water and energy are sufficiently available, the memory accumulation is much faster in earlier stages but then slows down in later stages. These findings are consistent with recent studies that have identified regime-dependent multi-timescale SMM and the regulation of it by hydro-climatic mechanisms, such as recharge frequency, evapotranspiration coupling and deep-storage buffering (Cinkus et al., 2023; Rahmati et al., 2024).

Table 2- Memory-related characteristics extracted from LIDE method for examined sites

https://doi.org/10.5194/egusphere-2026-549
Preprint. Discussion started: 4 February 2026

Variables	Energy-limited site [Rollesbroich]	Water-limited site [Selhuasen]	Intermediate site [Schöneseiffen]
Memory accumulation rates			
Frequency coefficient lambda [days^{-1}]	-0.132	-0.031	-0.323
Early slow-memory accumulation slope [days^{-1}]	0.090	-	0.139
Intermediate slow-memory accumulation slope [days^{-1}]	0.007	-0.023	0.003
Late slow-memory accumulation slope [days^{-1}]	1.158	0.814	0.775
Memory Saturation line slope [days^{-1}]	0.022	0.097	0.005
Memory timescales			
Fast-memory timescale τ_F [days]	7.6	32.4	3.1
Short-term slow-memory timescale τ_{SS} [days]	13	-	39
Intermediate-term slow-memory timescale τ_{MS} [days]	125	127	115
Long-term slow-memory timescale τ_{LS} [days]	291	541	218
Memory saturation timescale τ_{sat} [days]	3270	3230	5651
Memory strength			
Actual memory capacity ($\mathcal{K}_C$) [days^{-1}]	1.232	1.210	1.116
Estimated memory capacity ($\widehat{\mathcal{K}}_C$) [days^{-1}]	1.242	1.192	1.079
Residual saturation [%], $r_s = \left(\left\|\mathcal{K}_C - \widehat{\mathcal{K}}_C\right\|\right)/\mathcal{K}_C \times 100$	~ 0.7	~ 1.5	~ 3.5
Soil Moisture reemergence			
Mean saturation spread [days^{-1}]	15.99	9.67	16.46
Minimum saturation spread [days^{-1}]	5.91	4.25	9.23
Maximum saturation spread [days^{-1}]	35.20	17.83	31.55

The memory saturation stage also provides another additional information (in addition to τ_{Sat} and $\mathcal{K}_C$) characterized by saturation plateau spread (see light-blue shaded area in Fig. 4) which is larger at initial times of saturation and then decreases by time, holding a sine cycle with slightly oscillating pattern. The mean value and its range (maximum spread at initial steps and minimum spread at final steps of memory saturation) can be served as appropriate metric to quantify very-long slow-memory timescale occurring at years to decades timescales, mainly known as soil moisture reemergence (Kumar et al., 2019), a process in which subsurface moisture anomalies existing from previous seasons sporadically recouple with the surface, causing secondary persistence peaks in autocorrelation. We calculated the normalized "saturation spread" as a quantifier of the amplitude of residual long-lag fluctuations, with a fitted upper–lower envelope technique. The spread is larger for the energy-limited site, reflecting stronger seasonal reactivation of stored anomalies by recharge–discharge and vegetation feedback, while the plateau has a more subdued maximum at the water-limited site, consistent with weaker hydraulic coupling and atmospheric dominance. Such behavior falls in between those sites when considering it for the intermediate site, closer to the energy-limited site than the water-limited site.

https://doi.org/10.5194/egusphere-2026-549
Preprint. Discussion started: 4 February 2026

4.4. LIDE framework over sub-daily data

As previously also mentioned, the conceptualization provided in previous section is subject to the resolution of the data used for timescales characterization (e.g. daily, as discussed so far). The effects of sampling frequency on SMM characterization is also already well documented in literature (e.g., see the extensive review of this topic in Rahmati et al., 2024). In this section, therefore, we show how far the conceptualization provided before is also valid when LIDE framework is applied for data with higher (e.g., hourly) resolutions. This is important because using soil moisture data with different resolutions can involve or overlook different soil processes (e.g. sub-daily contribution of drainage which is usually overlooked at daily or monthly data) that could affect the memory at different components identified.

To test whether the LIDE framework can resolve sub-daily, short-term memory components, we applied LIDE to hourly soil moisture data from our Schöneseiffen site (see Fig. 5). This yielded a frequency coefficient λ value of -0.173 hours^{-1}, leading to a fast memory τ_F of 5.8 hours (see Table 3). Interestingly, this value is very close to that obtained by applying the hybrid stochastic–deterministic framework (McColl et al., 2019) — a classical method used in the literature — on the same data, but resampled at daily resolution ($\tau_S^H|_{\text{daily}} \approx 7.5$ hours; see Table 4). Similarly, the long-term memory captured by applying the hybrid stochastic–deterministic framework to daily data ($\tau_L^H|_{\text{daily}} \approx 32$ days; see Table 4) is also very close to the short-term memory captured by applying the LIDE framework to hourly data ($\tau_S|_{\text{hourly}} \approx 24$ days; see Table 3) and daily data ($\tau_S|_{\text{daily}} \approx 39$ days; see Table 3). These results remarkably suggest that when high-frequency data is available, the LIDE can capture the same rapid hydrological adjustments mechanistically as the hybrid model does empirically. In other words, as mentioned above, for the LIDE framework to be able to capture memory timescales at sub-daily scale, it requires high frequency hourly data, but the advantage is that it deterministically determines the shortest memory (fast memory) by λ and puts the memory at larger scales into distributed memory kernel, which can be decomposed by LPMS method. In other words, the hybrid stochastic–deterministic model can express sub-daily processes even based on daily data, yet this capability arises from the empirical nature with which parameterized stochastic terms effectively interpolate between unmodelled temporal scales. In contrast, the LIDE framework resolves the same short-term memory deterministically, via inclusion of an explicit relaxation term λ not associated with empirical interpolation. Additionally, the convolutional kernel in the LIDE framework inherently splits the long-scale dynamics into distributed memory domain and avoids timescale mixture, which is not possible with the hybrid stochastic–deterministic framework, which is elaborated more later.

The comparison of cumulative memory kernels obtained from hourly and daily data at Schöneseiffen site (Fig. 6) indicates an underlying resolution dependence on the representation of SMM. Daily sampling sums up sub-daily hydrological processes (rapid infiltration, diurnal evaporation cycles and shallow root uptake) into a single effective fast-memory mode that can be seen as a linear accumulation segment at short lags, followed by a single logistic transition at long time lags. Hourly sampling, however, captures separate dynamical processes operative at sub-daily, daily and multi-day timescales. This produces a very small linear segment at the smallest lags (which reflects true instantaneous decay), followed by two distinct logistic transitions for (i) sub-daily to daily-scale accumulation induced by diurnal forcing and shallow storage processes, and (ii) daily-to-

https://doi.org/10.5194/egusphere-2026-549
Preprint. Discussion started: 4 February 2026

seasonal accumulation regulated by deeper soil moisture storage. Accordingly, the hourly LIDE kernel exposes the physical multilayered structure of SMM, while daily data places these fast modes into an effective one-stage representation. Therefore, by application of LIDE framework over hourly data, we were able to identify one additional timescale —namely very-short-term slow-memory timescale τ_{VSS} — with a value of 14 hours for intermediate site which falls in between fast memory timescale ($\tau_F|_{\text{hourly}} \approx 5.8$ hours; see Table 3) and short-term slow memory timescale ($\tau_S|_{\text{hourly}} \approx 24$ days; see Table 3). Application of the LIDE framework to hourly and daily data further shows that an increase in temporal resolution mainly affects the fastest parts of SMM while the larger lag timescales remain unaffected. As expected, the hourly data lead to a significantly shorter τ_F value plus that an additional very-short slow-memory timescale (τ_{VSS}) is revealed. The latter was hidden at daily resolution because sub-daily infiltration-evaporation pulses and diurnal root-water-uptake dynamics were aliased in a single composite fast-relaxation parameter of daily data. In contrast, the slow-memory timescales (τ_{SS}, τ_{MS}, and τ_{LS}) and eventual saturation (τ_{Sat}) only moderately differ between hourly and daily analysis; τ_{SS} becomes shorter (39 → 23.8 days), whereas there is little change in τ_{MS} (115 → 128 days) and almost no change in τ_{LM} (218 → 214 days), with the saturation timescale being pretty much independent of scale (≈15 years). This pattern shows that the long-memory processes—seasonal recharge and deep percolation as well as vadose zone storage integration — operate on timescales far longer than the sampling interval and LIDE method can capture this nicely. Hence while high-frequency data are needed to tease out the sub-daily and short-term slow-memory components, the multi-month and multi-year memory structure of the soil system appears to be insensitive to temporal aggregation suggesting that LIDE is capturing the dominant slow-memory architecture even at daily scale. However, such behavior is not guaranteed by hybrid model where two completely different long-term memory obtained from hybrid method when applying on daily data (with $\tau_L^H|_{\text{daily}} \approx 32$ days; see Table 4) and hourly data (with $\tau_L^H|_{\text{hourly}} \approx 7.5$ days) confirms this argument.

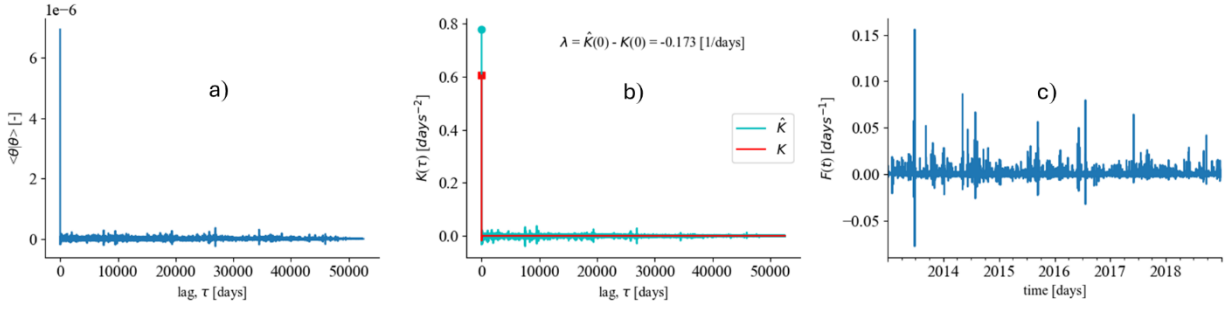

Figure 5 - The variation of LIDE framework parameters over time or lag domains, obtained from daily root-zone soil moisture (θ_{root}) signals at Schöneseiffen site. a) Autocorrelation function, ⟨θ|θ⟩, b) memory kernels K(τ) and $\widehat{K}(\tau)$, c) noise term F(t)

Table 3- Memory-related characteristics extracted from LIDE framework applied over hourly, daily, and monthly data in intermediate site (Schöneseiffen)

Variables	Hourly data	Daily data	Monthly data

https://doi.org/10.5194/egusphere-2026-549
Preprint. Discussion started: 4 February 2026

Memory accumulation rates§	-	-	-
Frequency coefficient lambda [T^{-1}]	-0.173	-0.323	-0.350
Very-early slow-memory accumulation slope [T^{-1}]	-0.030	-	-
Early slow-memory accumulation slope [T^{-1}]	0.225	0.139	-
Intermediate slow-memory accumulation slope [T^{-1}]	0.050	0.003	0.056
Late slow-memory accumulation slope [T^{-1}]	0.754	0.775	0.786
Memory Saturation line slope [T^{-1}]	0.005	0.005	0.042
Memory timescales	-	-	-
Fast-memory timescale τ_F [T]	5.78	3.10	2.86
Very short-term slow-memory timescale τ_{VSS} [hours]	14	-	-
Short-term slow-memory timescale τ_{SS} [days]	23.8	39	-
Intermediate-term slow-memory timescale τ_{MS} [days]	128	115	92
Long-term slow-memory timescale τ_{LS} [days]	214	218	336
Memory saturation timescale τ_{Sat} [years]	15.1	15.5	6.8
Memory strength	-	-	-
Actual memory capacity ($\mathcal{K}_C$) [$days^{-1}$]	1.26	1.12	1.13
Estimated memory capacity ($\widehat{\mathcal{K}_C}$) [$days^{-1}$]	1.23	1.08	1.13
Residual saturation [%], $r_S = \left(\left\|\mathcal{K}_C - \widehat{\mathcal{K}_C}\right\|\right)/\mathcal{K}_C \times 100$	2.59	3.35	0.41
Soil Moisture reemergence	-	-	-
Mean saturation spread [T^{-1}]	14.62	16.46	13.64
Minimum saturation spread [T^{-1}]	8.08	9.23	2.48
Maximum saturation spread [T^{-1}]	28.37	31.55	32.86

§: In the case of hourly data, T is 'hours'; for daily data, it is 'days'; and for monthly data, it is 'months'. To make the comparisons easier, we have converted (wherever possible) hourly timescales to daily by dividing by 24 and monthly timescales by multiplying by 30.5, which is the average number of days in a month within a 365-day year.

https://doi.org/10.5194/egusphere-2026-549
Preprint. Discussion started: 4 February 2026

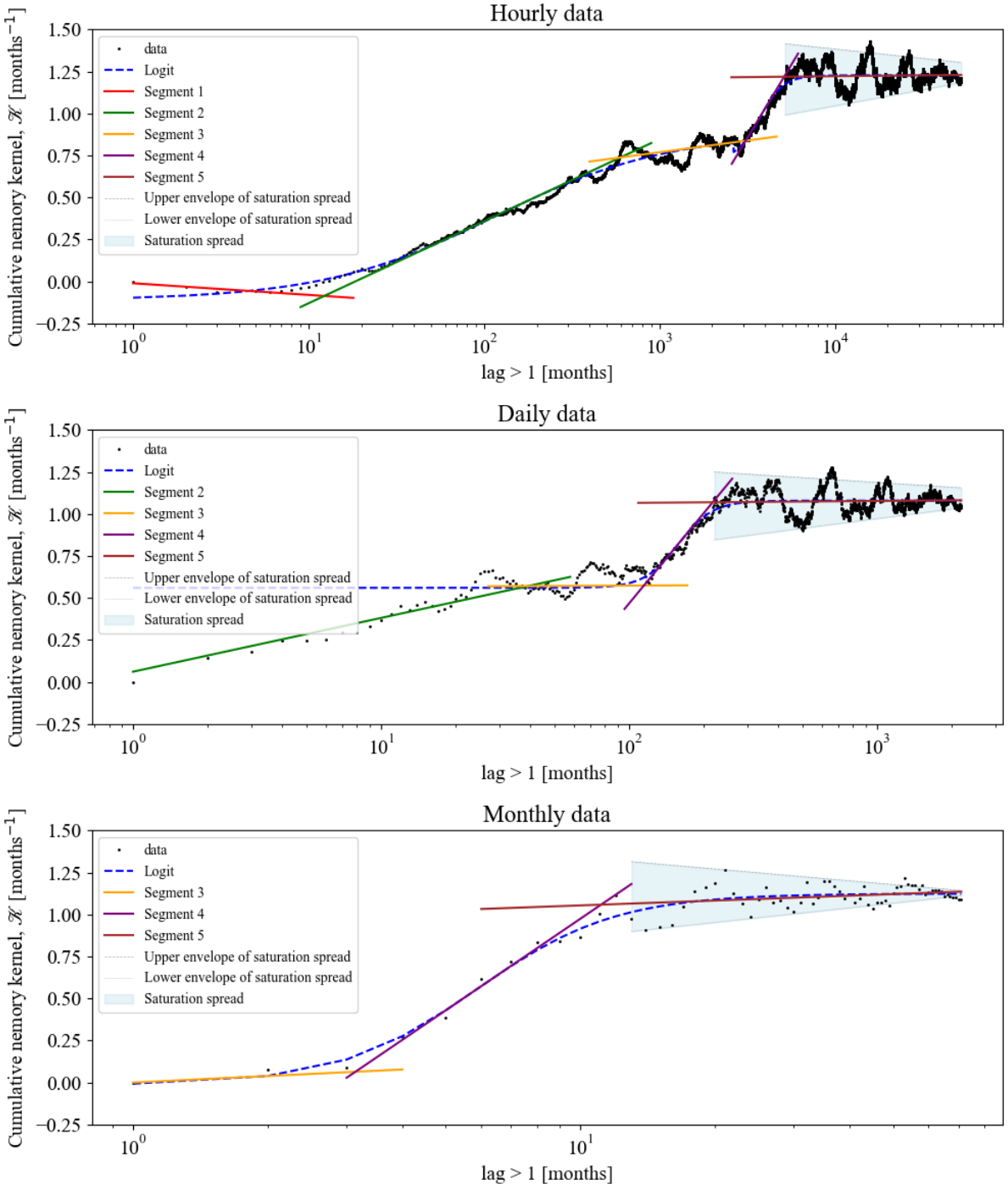

Figure 6 – Cumulative memory kernel $\mathcal{K}(\tau)$ for Schöneseiffen site obtained from application of LIDE framework over hourly, daily, and monthly data.

635

https://doi.org/10.5194/egusphere-2026-549
Preprint. Discussion started: 4 February 2026

4.5. LIDE framework over monthly data

When LIDE is used over monthly soil-moisture data, the shape (see Fig. 6) and interpretation (see Table 3) of the cumulative memory kernel change significantly. After resampling data at monthly frequency, all sub-seasonal variations are removed thereby eliminating the very-short-term and short-term slow-memory components (τ_{VSS} and τ_{SS}) that are detectable in hourly/daily data. In this way, the monthly kernel transits rapidly to intermediate and long-term memory regimes, yielding a shorter mid-term memory timescale (τ_{MS} = 92 days vs. 115 and 128 days observed in daily and hourly datasets; see Table 3) but lengthened long-term timescale (τ_{LS} = 336 days vs. 218 and 214 days observed in daily and hourly datasets; see Table 3). The time to saturation is also obviously compressed (τ_{Sat} ~ 6.8 years) compared to that of more than 15 years observed in both daily and hourly data, indicative of quick convergence toward the asymptote due to temporal averaging. Moreover, the reemergence-like oscillatory patterns that we observe in the daily and hourly data are heavily damped at monthly timescale resulting in lower saturation spread statistics and negligible amount of residual saturation. In contrast, even with these structural adjustments, the total memory capacity is largely comparable across resolutions (with $\mathcal{K}_C$ varying between 1.13 and 1.26; being slightly larger for hourly dataset; see Table 3) indicating that monthly sampling essentially redistributes memory between different timescales rather than changing the overall amount of memory stored in the soil system.

4.6. Relevance of LIDE-derived memory timescales with classical metrics

As already discussed earlier, the SMM in literature is classically characterized by the conventional time-lag autocorrelation of soil-moisture anomalies, with memory defined as the timescale at which the autocorrelation suppresses to its e-folding (Delworth and Manabe, 1988; Koster and Suarez, 2001; McColl, Wang, et al., 2017; Orth and Seneviratne, 2013). These procedures effectively assume an exponential decay in response (which corresponds to the integral or bulk memory of the system) which conceals the coexistence of several characteristic timescales due to different types of storage and flux processes is hidden (Cinkus et al., 2023; Miralles et al., 2019). More recently proposed hybrid stochastic–deterministic schemes (McColl et al., 2019) have helped alleviate this by introducing a “hybrid” or scale-separated representation of the land–atmosphere system comprising short-term SMM (τ_S^H) and long-term SMM (τ_L^H) timescales, but they are still empirical in nature. In contrast, the LIDE framework introduced here directly models memory from observed dynamics which decomposes it into an instantaneous relaxation process (fast term) and nonlocal slow-memory that accumulates over slower processes. Therefore, in this section, we compare SMM timescales inferred from LIDE to those of classical e-folding as well as hybrid stochastic–deterministic ones (see Table 4) in order to (i) test the numerical consistency of opposing memory estimates, (ii) understand their ability to reflect persistence at sub-seasonal and inter-annual scales, and (iii) explore how hydro-climatic regime-specificity affects apparent memory length across methods.

Although partly discussed in previous section, results reveal that there are methodological and regime-dependent differences between obtained memory timescales (Table 4). The classical e-folding analyses provide integral memory timescales of 52 days, 87 days, and 82 days for the energy-limited, water-limited, and intermediate sites, respectively — values typical of bulk persistence associated with exponential autocorrelation decay (Delworth and Manabe, 1988; Koster and Suarez, 2001; McColl,

https://doi.org/10.5194/egusphere-2026-549
Preprint. Discussion started: 4 February 2026

Wang, et al., 2017; Orth and Seneviratne, 2013). The hybrid stochastic–deterministic model resolves this behavior into a sub-daily short-term (with ~5 hours for both energy-limited and water limited sites and ~8 hours for intermediate site) and long-term memory (with 68, 84, and 32 days for energy-limited, water-limited, and intermediate sites, respectively) timescales. However, it is worth noting that the sub-daily signal results from empirical interpolation beyond the resolution of daily data and accordingly represent parameter extrapolation more than observed fast dynamics. Contrarily, the LIDE framework obtains deterministically both the instantaneous and distributed memory components out of the temporal evolution of time-series. The derived fast memory (τ_F = 7.6 days, 32.4 day, and 3.1 days; see Table 4) reflects resolvable short-term damping, whereas the subsequent slow-memory timescales (τ_{SS}, τ_{MS}, τ_{LS}) describe a continuum from sub-monthly (~2 weeks) to multi-annual (~541 days) persistence. The timescale of saturation (τ_{Sat}) ranges from 9 to 15.5 years, demonstrating the persistent factor of long-lag impacts especially under water-limited conditions. Together, these results demonstrate that LIDE accounts for the exponential persistence detected by classical metrics and for the dual-mode structure of hybrid models within a unified physically based framework and provides an interpretable decomposition of SMM across temporal scales and hydro-climatic conditions. Notably, the shorter fast memory at the energy-limited site and longer at the water-limited site is consistent in all examined methods, showing their agreement in capturing the underlaying mechanisms (Table 4). The separation of "fast" and "slow" terms in LIDE framework is consistent with a multi-timescale framework for SMM, wherein λ sets the rate for decay of anomalies in the active layer, and the distributed memory kernel captures slower subsurface and feedback-driven persistence.

Table 4- Memory timescales of daily soil moisture among various analytical approaches and hydrological conditions.

Timescales	Symbol	Energy-limited site (Rollesbroich)	Water-limited site (Selhausen)	Intermediate site (Schöneseiffen)
Classical e-folding method				
Memory timescale	τ	52 days	87 days	82 days
Hybrid stochastic-deterministic model				
Short-term memory	τ_S^H	4.95 hours	5.11 hours	7.54 hours
Long-term memory	τ_L^H	68 days	84 days	32 days
LIDE method				
Fast memory	τ_F	7.6 days	32.4 days	3.1 days
Short-term slow-memory	τ_{SS}	13.4 days	-	39.2 days
Intermediate slow-memory	τ_{MS}	125 days	127 days	115 days
Long-term slow-memory	τ_{LS}	291 days	541 days	218 days
Saturation	τ_{Sat}	~9 years	~9 years	~15.5 years
$\mathcal{K}_{10}$ slow-memory	τ_{10}	90 days	164 days	2 days
$\mathcal{K}_{50}$ slow-memory	τ_{50}	168 days	309 days	48 days
$\mathcal{K}_{90}$ slow-memory	τ_{90}	~1.5 years	~1.8 years	~2.1 years

https://doi.org/10.5194/egusphere-2026-549
Preprint. Discussion started: 4 February 2026

4.7. Additional quantile-based slow-memory timescales

In addition to the stage-oriented slow-memory timescales (identified as above), we also quantified (see Table 5) timescales at 10, 50, and 90 percent quantiles ($\mathcal{K}_{10}$, $\mathcal{K}_{50}$, and $\mathcal{K}_{90}$) of slow-memory accumulations — known as τ_{10}, τ_{50}, and τ_{90} — which present contrasting hydrologic fingerprints among the three sites. The τ_{10} values indicate that slow-memory accumulation is initiated earliest at the intermediate site (2 days), later at energy-limited site (90 days) and much later still at water-limited site (164 days). This behavior indicates that the intermediate site probably contains very responsive, shallow storage pathways (where neither water nor energy supplies are limiting factors), while for dryer sites the pathways are longer, and it requires longer time before deep-storage processes begin to contribute to memory. The differences among examined sites are clearer when comparing the τ_{50}, (halfway point of the total slow-memory accumulation): the intermediate site accumulates 50 % of its total memory within 48 days only, while it takes around half-year (168 days) for the energy-limited site and around one-year (309 days) for the water-limited site. This indicates that the dominant slow-memory operating timescale is site-dependent whereas it is shortest in the intermediate regime, moderate in the humid energy-limited site, and longest in the dry water-limited site. Finally, the τ_{90} values highlight these regime contrasts further where the energy-limited site accumulates 90% of its memory capacity in 1.3 years, while it takes around 1.8 years for the water-limited site and around 2 years for the intermediate site as a reflection of its highly distributed deep storage and long-tailed persistence. In general, our finding indicates that: (i) energy-limited site accumulates memory more evenly over time scales; (ii) water-limited site accumulates slow yet deep memories; and (iii) intermediate systems feature a swift initial build-up followed by an extended tail towards longer times, but probably this is site-specific subject to hydro-climate structure of the site and needs to be explored in other regions to gain an overall insight.

Table 5- Additional quantile-based slow-memory timescales extracted from LIDE method for examined sites.

Variables	Energy-limited site [Rollesbroich]	Water-limited site [Selhuasen]	Intermediate site [Schöneseiffen]
10% quantile ($\mathcal{K}_{10}$) slow-memory timescale τ_{10} [days]	90	164	2
50% quantile ($\mathcal{K}_{50}$) slow-memory timescale τ_{50} [days]	168	309	48
90% quantile ($\mathcal{K}_{90}$) slow-memory timescale τ_{90} [days]	489	672	759

4.8. Logistic representation and parameterization of the cumulative memory kernel

Finally, one might also describe the cumulative memory kernel for lags > 1 through the logistic function (see Methods) fitted over cumulative memory kernel. Calculated logistic coefficients (Table 6) exhibit systematic differences between examined regimes, confirming the already discussed differences in previous section. The energy-limited site has lower μ (= 191 days) and S (= 0.225 [-]) but somewhat higher $\widehat{\mathcal{K}}_C$ (≈ 1.24 days^{-1}), which suggests that memory accumulation at energy-limited site is more rapid yet more focused—the system reaches saturation rapidly within growing-season-constrained times and has relatively homogeneous hydrologic flow paths. In contrast, the water-limited site is characterized by larger μ (= 277 days) and S (= 0.409 [-]) values and a smaller $\widehat{\mathcal{K}}_C$ (≈ 1.19 days^{-1}), reflecting slower, more diffusive accumulation over a heterogeneous

https://doi.org/10.5194/egusphere-2026-549
Preprint. Discussion started: 4 February 2026

soil–vegetation system. The intermediate site, in line with what discussed in previous section, shows even faster memory accumulation (faster than energy-limited site) with smaller μ (= 158 days), smaller S (= 0.16 [-]), and smaller $\widehat{\mathcal{K}}_C$ (≈ 1.08 days^{-1}). These differences further emphasize that the logistic description adequately accounts for regime-dependent SMM organization: relatively contracted and strongly seasonally modulated in energy-limiting conditions, versus diffusive and multiannual in water-limited conditions.

Table 6- Logistic functions parameters obtained for examined sites.

Variables	Energy-limited site [Rollesbroich]	Water-limited site [Selhuasen]	Intermediate site [Schöneseiffen]
Baseline cumulative memory - α [1/days]	0.194	-0.152	0.560
Total memory capacity - β [1/days]	1.048	1.343	0.519
Estimated memory capacity - $\widehat{\mathcal{K}}_C = \alpha + \beta$	1.242	1.192	1.079
Characteristic memory lag - μ [days]	191	277	158
Active memory spread - S [-]	0.225	0.409	0.160
Logit function fitting accuracy [R]	0.975	0.992	0.888

5. Conclusions

This study developed a comprehensive and mechanistically interpretable framework, and scale-aware Linear Integro-Differential Equation (LIDE) for root-zone soil moisture which can quantitatively evaluate full-spectrum soil moisture memory (SMM) behavior in fast, slow, and very long-term timescales. By estimating a continuous distributed memory kernel from observations, LIDE is free of the prevalent shortcomings faced by classical memory diagnostics based on e-folding decay (Delworth and Manabe, 1988; Koster and Suarez, 2001; McColl, Wang, et al., 2017; Orth and Seneviratne, 2013) or hybrid stochastic-deterministic model (McColl et al., 2019) that inevitably compress the system's intricate temporal dynamics into one or at most two characteristic timescales. By applying automated Logit–Piecewise Memory Segmentation (LPMS) method to decompose the slow-memory component of LIDE framework, our analysis shows that LIDE not only recovers the traditional short- and long-term memory components but also reveals multiple different slow-memory regimes representing distinct hydrological processes and storage responses. This includes very-short-term (at sub-daily scale, in case of hourly data), short-term (on the order of weeks), mid-term (months to seasons), long-term (seasonal to years), and saturation (multi-year) memory regimes, allowing a unique multiscale decomposition of ecohydrological memory heretofore unattainable using classical methodologies. Such a multiscale identification is important because different memory modes control fundamentally distinct processes and feedback, important for land–atmosphere coupling and flash-drought evolution, e.g., soil-moisture anomalies lead to extreme drought warning (Liang and Yuan, 2021), vegetation resilience, soil–plant water use, and ecosystem carryover (Groh et al., 2020), among the others.

Across the three contrasting hydro-climatic regimes (water-limited, energy-limited, and intermediate sites), LIDE found that fast-memory differed by an order of magnitude (3–32 days), while short- and mid-term slow-memory were quite similar (τ_{SS}

https://doi.org/10.5194/egusphere-2026-549
Preprint. Discussion started: 4 February 2026

≈ 13–39 days; τ_{MS} ≈ 115–128 days), long-term memory timescale and time scale to saturation diverged drastically (τ_{LS} ≈ 218–541 days and τ_{Sat} ≈ 9-15 years). Another methodological advance is that LIDE provides information about memory strength/capacity as well and not only on timescale(s). Traditional methods measure the persistence of anomalies, but do not describe how powerfully previous states control future water availability. The LIDE kernel allows direct estimation of total memory capacity ($\mathcal{K}_C$): with $\mathcal{K}_C$ differing slightly from 1.12 −1.24 days^{-1}. This dual characterization—memory timescale and strength—provides a more comprehensive measurement of soil–plant–atmosphere interactions that is important for drought propagation, ecosystem resilience or coupled land-atmosphere feedback (Canarini et al., 2021; Rahmati et al., 2024; Schumacher et al., 2022; Seneviratne et al., 2010). For example, these results demonstrate that examined sites with contrasting hydro-climate regimes differ primarily in the distribution of memory across timescales, rather than their overall ability to retain past moisture anomalies.

The LIDE framework also quantitatively diagnoses, for the first time in field data, soil-moisture reemergence (Kumar et al., 2019) as part of SMM modes—a phenomenon previously documented very rarely and is overlooked mainly. Fluctuations of the saturation plateau in cumulative kernel are indicative of seasonally developing anomalies in storage; most pronounced in systems that are energy-limited (possibly with a strong recharge during wintertime and activation of deep storage). Through the identification of upper and lower envelopes to these oscillations, LIDE provides an objective assessment of reemergence, amplitude, spread and duration—quantities that previously could not be obtained in situ.

We evaluated the scale-awareness of LIDE by applying it over data at different temporal resolutions (hourly, daily, monthly). Such a comparison revealed that LIDE is structurally robust to the frequency of data in medium- and long-lag processes but detects short-term patterns more detailed when higher-frequency data is available. This shows that LIDE indeed represents hydrologically meaningful behavior rather than artefacts of the sampling resolution.

In general, the LIDE framework along with its helper function of LPMS described in this paper is a state-of-the-art and state-of-practice technique to diagnose the SMM. With its high physical interpretability and comprehensive multiscale characterization, including fast memory, multiple slow-memory compartments, memory strength/capacity, saturation behavior, and reemergence, LIDE offers a much richer (and more mechanistic) view of land-surface memory compared to classical approaches. This capability positions LIDE as a cornerstone for ongoing research on hydrologic predictability, drought evolution, land-atmosphere coupling and ecohydrological risk, and paves the way to standardized memory diagnostics in Earth-system modeling and environmental monitoring.

The main advantages of LIDE, beyond the clear advancements in SMM multi-timescales quantification skill, is that it bundles the drivers of θ_{root} dynamics into a parsimonious number of terms that effectively capture the reversible and irreversible changes in θ_{root} while requiring less detailed information about soil heterogeneity, vegetation dynamics, and root architecture as well as atmospheric forcings. Such a reduction enables us to make our proposed framework to be scale-aware, which can be applied at different scales.

Besides the advancements presented above, future work on further development of the LIDE framework can have several exciting directions. First, through extensive observational networks and satellite products, LIDE could be applied to developing

https://doi.org/10.5194/egusphere-2026-549
Preprint. Discussion started: 4 February 2026

a spatially varying map of multi-scale SMM, which would facilitate an investigation into how memory regimes vary with climate, soil and vegetation. Second, parameterization of the cumulative kernel in terms of a logistic function offers an efficient parametric description of distributed memory and hence the possibility to develop pedotransfer-type models that associate the parameters of logistic function with soil properties, vegetation traits and climate characteristic; a route toward operationalizing diagnostics of memory in land surface or drought-forecasting models. Third, the incorporation of LIDE in land-surface models and data assimilation systems can potentially enhance hydrologic predictability by explicitly assigning a diagnostic and corrective role to memory error terms inherent to model structure. Lastly, the capacity of LIDE to interpret oscillatory saturation behavior provides a new route for investigating soil-moisture reemergence and its connection with seasonal charge, freeze-thaw processes and ecosystem recovery. Collectively, such indications suggest that LIDE may develop into an ongoing integral diagnostic and predictive source for hydrology, drought science, and land-atmosphere studies.

Finally, while LIDE offers a detailed and physically interpretable description of multiscale SMM, there are also limitations that need to be acknowledged. First, the approach depends on relatively long and continuous time series—its ability to distinguish between memory regimes is influenced by temporal resolution and the coverage in time of the data set. Ideally, the data retention period should be longer than the memory saturation phase onset (i.e. more than a year). Second, LIDE assumes a linear convolutional structure for the (potentially) nonlinear process and heavily nonlinear processes such as preferential flow, hysteresis in infiltration dynamics or state-dependent vegetation responses may be partially aliased into the estimated kernel by using this assumption. Third, kernel estimation may be data-sensitive, especially for noise and lags at shorter timescales, and thus needs to be regularized carefully along with the uncertainty quantification. Fourth, the convolution of forcings are intentionally added into noise term to make the numerical solution developed by Schmitt and Schulz (2006) applicable also here. One can keep those forcings separated by advancing such numerical solution. The physical interpretation of negative kernel lobes or multimodal signatures must also be treated with caution, as these also may be due to both real hydrological mechanisms and artifacts of aggregation or covariance structure. These limitations do not diminish LIDE diagnostic value but rather indicate the direction in which methodological improvement and supplementary analyses will enhance its utility.

Code and data availability

The data used in this analysis will be made available publicly upon acceptance of the paper. The code used in this analysis will be made available publicly through GitHub repository upon acceptance of the paper.

Conflict of Interest Disclosure

The authors declare there are no conflicts of interest in this manuscript.

Competing interests

The authors declare that they have no conflict of interest.

https://doi.org/10.5194/egusphere-2026-549
Preprint. Discussion started: 4 February 2026

Disclaimer

Copernicus Publications remains neutral regarding jurisdictional claims made in the text, published maps, institutional affiliations, or any other geographical representation in this paper. While Copernicus Publications makes every effort to include appropriate place names, the final responsibility lies with the authors. Views expressed in the text are those of the authors and do not necessarily reflect the views of the publisher.

Acknowledgements

The author thanks with pleasure his numerous colleagues for their precious help and stimulating discussions during the entire work. Notably, Prof. Dr. Harry Vereecken and Prof. Dr Jan Vanderborght provided insightful input during the early stages of conception of the method which enhanced immensely both the coherence and scientific content presented in here. The author also greatly appreciated important discussions with researchers and colleagues at several conferences, workshops, and seminars during research that helped to sharpen the interpretations and broaden the methodological viewpoint.

References

Abdoli, S., Rahmati, M., Ahmadi, H., Kamali, B., Groh, J., and Vereecken, H.: Interplay of soil moisture memory and soil hysteresis, Authorea Preprints, doi: https://doi.org/10.22541/essoar.173456507.72275820/v1, 2024. 2024.

Aldrees, A. and Nachabe, M.: Capillary Length and Field Capacity in Draining Soil Profiles, Water Resources Research, 55, 4499-4507, 2019.

Amenu, G. G., Kumar, P., and Liang, X. Z.: Interannual variability of deep-layer hydrologic memory and mechanisms of its influence on surface energy fluxes, Journal of Climate, 18, 5024-5045, 2005.

Bevacqua, E., Rakovec, O., Schumacher, D. L., Kumar, R., Thober, S., Samaniego, L., Seneviratne, S. I., and Zscheischler, J.: Direct and lagged climate change effects intensified the 2022 European drought, Nature Geoscience, 17, 1100-1107, 2024.

Boden, A.: Ad-hoc-AG Boden, Bodenkundliche Kartieranleitung, Aufl., Hannover, 2005. 2005.

Bogena, H., Montzka, C., Huisman, J., Graf, A., Schmidt, M., Stockinger, M., Von Hebel, C., Hendricks-Franssen, H., Van der Kruk, J., and Tappe, W.: The TERENO-Rur hydrological observatory: A multiscale multi-compartment research platform for the advancement of hydrological science, Vadose Zone Journal, 17, 1-22, 2018.

Bogena, H., Schrön, M., Jakobi, J., Ney, P., Zacharias, S., Andreasen, M., Baatz, R., Boorman, D., Duygu, B. M., and Eguibar-Galán, M. A.: COSMOS-Europe: a European network of cosmic-ray neutron soil moisture sensors, Earth System Science Data, 14, 1125-1151, 2022.

Buckley, T. N.: How do stomata respond to water status?, New Phytologist, 224, 21-36, 2019.

https://doi.org/10.5194/egusphere-2026-549
Preprint. Discussion started: 4 February 2026

Calabritto, M., Mininni, A. N., Di Biase, R., Pietrafesa, A., and Dichio, B.: Spatio-temporal dynamics of root water uptake and identification of soil moisture thresholds for precision irrigation in a Mediterranean yellow-fleshed kiwifruit orchard, Frontiers in Plant Science, 15, 1472093, 2024.

Canarini, A., Schmidt, H., Fuchslueger, L., Martin, V., Herbold, C. W., Zezula, D., Gündler, P., Hasibeder, R., Jecmenica, M., Bahn, M., and Richter, A.: Ecological memory of recurrent drought modifies soil processes via changes in soil microbial community, Nature Communications, 12, 5308, 2021.

Cinkus, G., Wunsch, A., Mazzilli, N., Liesch, T., Chen, Z., Ravbar, N., Doummar, J., Fernández-Ortega, J., Barberá, J. A., Andreo, B., Goldscheider, N., and Jourde, H.: Comparison of artificial neural networks and reservoir models for simulating karst spring discharge on five test sites in the Alpine and Mediterranean regions, Hydrol. Earth Syst. Sci., 27, 1961-1985, 2023.

Cleverly, J., Eamus, D., Coupe, N. R., Chen, C., Maes, W., Li, L., Faux, R., Santini, N. S., Rumman, R., and Yu, Q.: Soil moisture controls on phenology and productivity in a semi-arid critical zone, Science of the Total Environment, 568, 1227-1237, 2016.

Delworth, T. L. and Manabe, S.: The Influence of Potential Evaporation on the Variabilities of Simulated Soil Wetness and Climate, Journal of Climate, 1, 523-547, 1988.

Falkena, S. K., Quinn, C., Sieber, J., Frank, J., and Dijkstra, H. A.: Derivation of delay equation climate models using the Mori-Zwanzig formalism, Proceedings of the Royal Society A, 475, 20190075, 2019.

Farmani, M. A., Behrangi, A., Gupta, A., Tavakoly, A., Geheran, M., and Niu, G.-Y.: Do land models miss key soil hydrological processes controlling soil moisture memory?, Hydrology and Earth System Sciences, 29, 547–566, 2025.

Gao, H., Hrachowitz, M., Schymanski, S., Fenicia, F., Sriwongsitanon, N., and Savenije, H.: Climate controls how ecosystems size the root zone storage capacity at catchment scale, Geophysical Research Letters, 41, 7916-7923, 2014.

Ghannam, K., Nakai, T., Paschalis, A., Oishi, C. A., Kotani, A., Igarashi, Y., Kumagai, T., and Katul, G. G.: Persistence and memory timescales in root-zone soil moisture dynamics, Water Resources Research, 52, 1427-1445, 2016.

Gómez, D. G., Ochoa, C. G., Godwin, D., Tomasek, A. A., and Zamora Re, M. I.: Soil Moisture and Water Transport through the Vadose Zone and into the Shallow Aquifer: Field Observations in Irrigated and Non-Irrigated Pasture Fields, Land, 11, 2029, 2022.

Gottwald, G. A., Crommelin, D. T., and Franzke, C. L.: Stochastic climate theory, arXiv preprint arXiv:1612.07474, 2016. 2016.

Gouasmi, A., Parish, E. J., and Duraisamy, K.: A priori estimation of memory effects in reduced-order models of nonlinear systems using the Mori–Zwanzig formalism, Proceedings of the Royal Society A: Mathematical, Physical and Engineering Sciences, 473, 20170385, 2017.

Groh, J., Vanderborght, J., Putz, T., Vogel, H. J., Gründling, R., Rupp, H., Rahmati, M., Sommer, M., Vereecken, H., and Gerke, H. H.: Responses of soil water storage and crop water use efficiency to changing climatic conditions: a lysimeter-based space-for-time approach, Hydrology and Earth System Sciences, 24, 1211-1225, 2020.

https://doi.org/10.5194/egusphere-2026-549
Preprint. Discussion started: 4 February 2026

Guo, J. S. and Ogle, K.: Antecedent soil water content and vapor pressure deficit interactively control water potential in Larrea tridentata, New Phytologist, 221, 218-232, 2019.

Han, J. and Zhou, Z.: Dynamics of soil water evaporation during soil drying: laboratory experiment and numerical analysis, The Scientific World Journal, 2013, 240280, 2013.

Hasselmann, K.: Stochastic climate models part I. Theory, Tellus, 28, 473-485, 1976.

Iden, S. C., Blöcher, J. R., Diamantopoulos, E., and Durner, W.: Capillary, film, and vapor flow in transient bare soil evaporation (1): Identifiability analysis of hydraulic conductivity in the medium to dry moisture range, Water Resources Research, 57, e2020WR028513, 2021.

Irvine, D. J., Singha, K., Kurylyk, B. L., Briggs, M. A., Sebastian, Y., Tait, D. R., and Helton, A. M.: Groundwater-Surface water interactions research: Past trends and future directions, Journal of Hydrology, 644, 132061, 2024.

Jacobs, E. M., Bertassello, L. E., and Rao, P. S. C.: Drivers of regional soil water storage memory and persistence, Vadose Zone Journal, 19, e20050, 2020.

Kaisermann, A., de Vries, F. T., Griffiths, R. I., and Bardgett, R. D.: Legacy effects of drought on plant–soil feedbacks and plant–plant interactions, New Phytologist, 215, 1413-1424, 2017.

Kargas, G., Soulis, K. X., and Kerkides, P.: Implications of hysteresis on the horizontal soil water redistribution after infiltration, Water, 13, 2773, 2021.

Knapp, J. L. A., Berghuijs, W. R., Floriancic, M. G., and Kirchner, J. W.: Catchment hydrological response and transport are affected differently by precipitation intensity and antecedent wetness, Hydrol. Earth Syst. Sci., 29, 3673-3685, 2025.

Kollet, S. J. and Maxwell, R. M.: Capturing the influence of groundwater dynamics on land surface processes using an integrated, distributed watershed model, Water Resources Research, 44, 2008.

Koster, R. D., Guo, Z. C., Yang, R. Q., Dirmeyer, P. A., Mitchell, K., and Puma, M. J.: On the Nature of Soil Moisture in Land Surface Models, Journal of Climate, 22, 4322-4335, 2009.

Koster, R. D., Mahanama, P., and Sarith, P.: Land surface controls on hydroclimatic means and variability, Journal of Hydrometeorology, 13, 1604-1620, 2012.

Koster, R. D. and Suarez, M. J.: Soil moisture memory in climate models, Journal of Hydrometeorology, 2, 558-570, 2001.

Kumar, S., Newman, M., Wang, Y., and Livneh, B.: Potential reemergence of seasonal soil moisture anomalies in North America, Journal of Climate, 32, 2707-2734, 2019.

Laio, F., Porporato, A., Ridolfi, L., and Rodriguez-Iturbe, I.: Plants in water-controlled ecosystems: active role in hydrologic processes and response to water stress: II. Probabilistic soil moisture dynamics, Advances in water resources, 24, 707-723, 2001.

https://doi.org/10.5194/egusphere-2026-549
Preprint. Discussion started: 4 February 2026

Lehmann, P. and Or, D.: Analytical model for bare soil evaporation dynamics following wetting with concurrent internal drainage, Journal of Hydrology, 631, 130800, 2024.

Li, B., Sprenger, M., Wyatt, B. M., Giménez, D., Hirmas, D. R., Ajami, H., Wiekenkamp, I., Groh, J., Nimmo, J. R., and Amato, M. T.: Ubiquity and causes of soil water preferential flow across 17 ecoregions, Geophysical Research Letters, 52, e2025GL118045, 2025.

Liang, M. L. and Yuan, X.: Critical Role of Soil Moisture Memory in Predicting the 2012 Central United States Flash Drought, Frontiers in Earth Science, 9, 615969, 2021.

Liu, Y., Xiao, J., Li, X., and Li, Y.: Critical soil moisture detection and water-energy limit shift attribution using satellite-based water and carbon fluxes over China, Hydrology and Earth System Sciences Discussions, 2024, 1-30, 2024.

Martínez-de la Torre, A. and Miguez-Macho, G.: Groundwater influence on soil moisture memory and land–atmosphere fluxes in the Iberian Peninsula, Hydrology and Earth System Sciences, 23, 4909-4932, 2019.

McColl, K. A., Alemohammad, S. H., Akbar, R., Konings, A. G., Yueh, S., and Entekhabi, D.: The global distribution and dynamics of surface soil moisture, Nature Geoscience, 10, 100-+, 2017.

McColl, K. A., He, Q., Lu, H., and Entekhabi, D.: Short-Term and Long-Term Surface Soil Moisture Memory Time Scales Are Spatially Anticorrelated at Global Scales, Journal of Hydrometeorology, 20, 1165-1182, 2019.

McColl, K. A., Wang, W., Peng, B., Akbar, R., Gianotti, D. J. S., Lu, H., Pan, M., and Entekhabi, D.: Global characterization of surface soil moisture drydowns, Geophysical Research Letters, 44, 3682-3690, 2017.

Miguez-Macho, G. and Fan, Y.: The role of groundwater in the Amazon water cycle: 2. Influence on seasonal soil moisture and evapotranspiration, Journal of Geophysical Research: Atmospheres, 117, 2012.

Miralles, D. G., Gentine, P., Seneviratne, S. I., and Teuling, A. J.: Land-atmospheric feedbacks during droughts and heatwaves: state of the science and current challenges, Ann N Y Acad Sci, 1436, 19-35, 2019.

Miralles, D. G., Holmes, T. R. H., De Jeu, R. A. M., Gash, J. H., Meesters, A. G. C. A., and Dolman, A. J.: Global land-surface evaporation estimated from satellite-based observations, Hydrology and Earth System Sciences, 15, 453-469, 2011.

Morbidelli, R., Corradini, C., Saltalippi, C., Flammini, A., and Rossi, E.: Infiltration-soil moisture redistribution under natural conditions: experimental evidence as a guideline for realizing simulation models, Hydrology and Earth System Sciences, 15, 2937-2945, 2011.

Mori, H.: Transport, collective motion, and Brownian motion, Progress of theoretical physics, 33, 423-455, 1965.

Mu, M., De Kauwe, M. G., Ukkola, A. M., Pitman, A. J., Guo, W., Hobeichi, S., and Briggs, P. R.: Exploring how groundwater buffers the influence of heatwaves on vegetation function during multi-year droughts, Earth System Dynamics Discussions, 2021, 1-29, 2021.

https://doi.org/10.5194/egusphere-2026-549
Preprint. Discussion started: 4 February 2026

Müller, L. M. and Bahn, M.: Drought legacies and ecosystem responses to subsequent drought, Global Change Biology, 28, 5086-5103, 2022.

Nimmo, J. R., Wiekenkamp, I., Araki, R., Groh, J., Singh, N. K., Crompton, O., Wyatt, B. M., Ajami, H., Giménez, D., and Hirmas, D. R.: Identifying preferential flow from soil moisture time series: Review of methodologies, Vadose Zone Journal, 24, e70017, 2025.

Or, D., Lehmann, P., Shahraeeni, E., and Shokri, N.: Advances in soil evaporation physics—A review, Vadose Zone Journal, 12, vzj2012. 0163, 2013.

Orozco-López, E., Muñoz-Carpena, R., Gao, B., and Fox, G. A.: Riparian Vadose Zone Preferential Flow: Review of Concepts, Limitations, and Perspectives, Vadose Zone Journal, 17, 180031, 2018.

Orth, R. and Seneviratne, S. I.: Predictability of soil moisture and streamflow on subseasonal timescales: A case study, Journal of Geophysical Research: Atmospheres, 118, 10,963-910,979, 2013.

Pales, A. R., Li, B., Clifford, H. M., Kupis, S., Edayilam, N., Montgomery, D., Liang, W. Z., Dogan, M., Tharayil, N., Martinez, N., Moysey, S., Powell, B., and Darnault, C. J. G.: Preferential flow systems amended with biogeochemical components: imaging of a two-dimensional study, Hydrol. Earth Syst. Sci., 22, 2487-2509, 2018.

Pütz, T., Kiese, R., Wollschläger, U., Groh, J., Rupp, H., Zacharias, S., Priesack, E., Gerke, H., Gasche, R., and Bens, O.: TERENO-SOILCan: a lysimeter-network in Germany observing soil processes and plant diversity influenced by climate change, Environmental Earth Sciences, 75, 1-14, 2016.

Rahmati, M., Amelung, W., Brogi, C., Dari, J., Flammini, A., Bogena, H., Brocca, L., Chen, H., Groh, J., Koster, R. D., McColl, K. A., Montzka, C., Moradi, S., Rahi, A., Sharghi S., F., and Vereecken, H.: Soil Moisture Memory: State-Of-The-Art and the Way Forward, Reviews of Geophysics, 62, e2023RG000828, 2024.

Rahmati, M., Graf, A., Poppe Terán, C., Amelung, W., Dorigo, W., Franssen, H.-J. H., Montzka, C., Or, D., Sprenger, M., and Vanderborght, J.: Continuous increase in evaporative demand shortened the growing season of European ecosystems in the last decade, Communications Earth & Environment, 4, 236, 2023.

Rahmati, M., Groh, J., Graf, A., Pütz, T., Vanderborght, J., and Vereecken, H.: On the impact of increasing drought on the relationship between soil water content and evapotranspiration of a grassland, Vadose Zone Journal, 19, e20029, 2020.

Rahmati, M., Or, D., Amelung, W., Bauke, S. L., Bol, R., Hendricks Franssen, H.-J., Montzka, C., Vanderborght, J., and Vereecken, H.: Soil is a living archive of the Earth system, Nature Reviews Earth & Environment, 4, 421-423, 2023.

Richards, L. A.: CAPILLARY CONDUCTION OF LIQUIDS THROUGH POROUS MEDIUMS, Physics, 1, 318-333, 1931.

Richardson, L. F.: Weather prediction by numerical process, University Press, 1922.

Schmitt, D. T. and Schulz, M.: Analyzing memory effects of complex systems from time series, Physical Review E, 73, 056204, 2006.

https://doi.org/10.5194/egusphere-2026-549
Preprint. Discussion started: 4 February 2026

Schumacher, D. L., Keune, J., Dirmeyer, P., and Miralles, D. G.: Drought self-propagation in drylands due to land–atmosphere feedbacks, Nature Geoscience, 15, 262-268, 2022.

Seneviratne, S. I., Corti, T., Davin, E. L., Hirschi, M., Jaeger, E. B., Lehner, I., Orlowsky, B., and Teuling, A. J.: Investigating soil moisture-climate interactions in a changing climate: A review, Earth-Science Reviews, 99, 125-161, 2010.

Seneviratne, S. I. and Koster, R. D.: A Revised Framework for Analyzing Soil Moisture Memory in Climate Data: Derivation and Interpretation, Journal of Hydrometeorology, 13, 404-412, 2012.

Seo, E., Dirmeyer, P. A., Barlage, M., Wei, H., and Ek, M.: Evaluation of Land–Atmosphere Coupling Processes and Climatological Bias in the UFS Global Coupled Model, Journal of Hydrometeorology, 25, 161-175, 2024.

Song, S. and Wang, W.: Impacts of Antecedent Soil Moisture on the Rainfall-Runoff Transformation Process Based on High-Resolution Observations in Soil Tank Experiments, Water, 11, 296, 2019.

Stacke, T. and Hagemann, S.: Lifetime of soil moisture perturbations in a coupled land–atmosphere simulation, Earth Syst. Dynam., 7, 1-19, 2016.

Stahl, M. O. and McColl, K. A.: The seasonal cycle of surface soil moisture, Journal of Climate, 2022. 1-35, 2022.

Teuling, A. J., Hirschi, M., Ohmura, A., Wild, M., Reichstein, M., Ciais, P., Buchmann, N., Ammann, C., Montagnani, L., Richardson, A. D., Wohlfahrt, G., and Seneviratne, S. I.: A regional perspective on trends in continental evaporation, Geophysical Research Letters, 36, 2009.

Thayamkottu, S., Masta, M., Skeeter, J., Pärn, J., Knox, S. H., Smallman, T. L., and Mander, Ü.: Dual controls of vapour pressure deficit and soil moisture on photosynthesis in a restored temperate bog, Science of the Total Environment, 963, 178366, 2025.

Thomas, C. K., Law, B. E., Irvine, J., Martin, J. G., Pettijohn, J. C., and Davis, K. J.: Seasonal hydrology explains interannual and seasonal variation in carbon and water exchange in a semiarid mature ponderosa pine forest in central Oregon, Journal of Geophysical Research: Biogeosciences, 114, 2009.

Van Loon, A. F., Kchouk, S., Matanó, A., Tootoonchi, F., Alvarez-Garreton, C., Hassaballah, K. E. A., Wu, M., Wens, M. L. K., Shyrokaya, A., Ridolfi, E., Biella, R., Nagavciuc, V., Barendrecht, M. H., Bastos, A., Cavalcante, L., de Vries, F. T., Garcia, M., Mård, J., Streefkerk, I. N., Teutschbein, C., Tootoonchi, R., Weesie, R., Aich, V., Boisier, J. P., Di Baldassarre, G., Du, Y., Galleguillos, M., Garreaud, R., Ionita, M., Khatami, S., Koehler, J. K. L., Luce, C. H., Maskey, S., Mendoza, H. D., Mwangi, M. N., Pechlivanidis, I. G., Ribeiro Neto, G. G., Roy, T., Stefanski, R., Trambauer, P., Koebele, E. A., Vico, G., and Werner, M.: Review article: Drought as a continuum – memory effects in interlinked hydrological, ecological, and social systems, Nat. Hazards Earth Syst. Sci., 24, 3173-3205, 2024.

Wang, Y., Gao, L., Li, J., and Peng, X.: Responses of deep soil moisture to direct rainfall and groundwater in the red soil critical zone: A four-stage pattern, Journal of Hydrology, 632, 130864, 2024.

Zhang, Y., Wei, H., and Nearing, M. A.: Effects of antecedent soil moisture on runoff modeling in small semiarid watersheds of southeastern Arizona, Hydrol. Earth Syst. Sci., 15, 3171-3179, 2011.

https://doi.org/10.5194/egusphere-2026-549
Preprint. Discussion started: 4 February 2026

Zhang, Y., Zhang, Z., Ma, Z., Chen, J., Akbar, J., Zhang, S., Che, C., Zhang, M., and Cerdà, A.: A review of preferential water flow in soil science, Canadian Journal of Soil Science, 98, 604-618, 2018.

Zwanzig, R.: Nonlinear generalized Langevin equations, Journal of Statistical Physics, 9, 215-220, 1973.

995